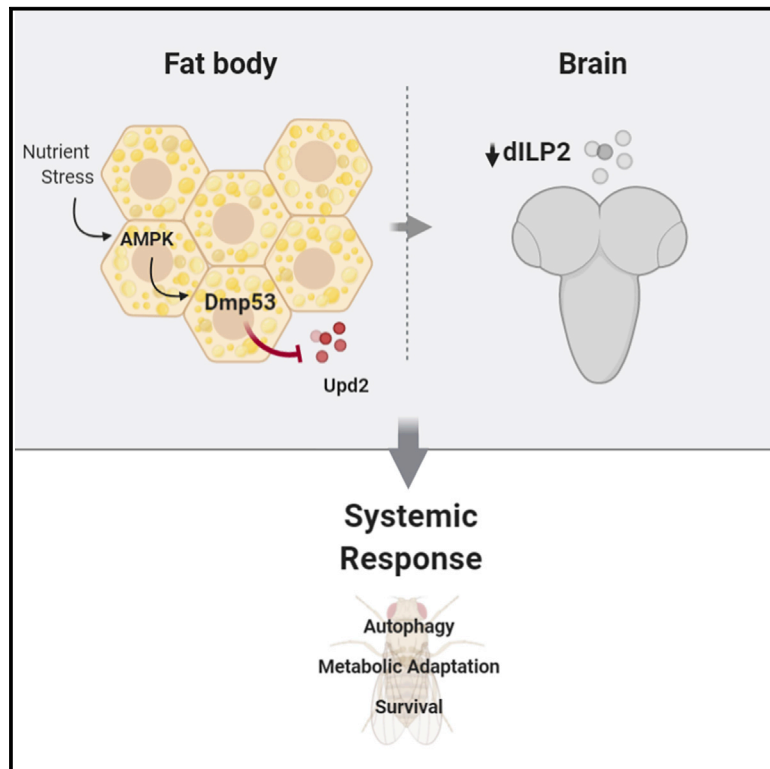Article

Fat Body p53 Regulates Systemic Insulin Signaling and Autophagy under Nutrient Stress via *Drosophila* Upd2 Repression

Graphical Abstract

Authors

María Clara Ingaramo,
Juan Andrés Sánchez, Norbert Perrimon,
Andrés Dekanty

Correspondence

perrimon@genetics.med.harvard.edu
(N.P.),
adekanty@santafe-conicet.gov.ar (A.D.)

In Brief

Ingaramo et al. report an essential role for adipose p53 in sensing nutrient stress, maintaining metabolic homeostasis, and extending organismal survival in *Drosophila*. AMPK-dependent Dmp53 activation under nutrient stress modulates Dilp2 circulating levels, systemic insulin/TOR signaling, and autophagy induction by repressing Leptin/Upd2 expression in adipose cells.

Highlights

- Adipose AMPK-p53 axis is required for *Drosophila* survival to nutrient stress

- Adipose Dmp53 represses Leptin/Upd2 expression, which remotely controls Dilp2 secretion

- Dmp53 activation regulates autophagy induction upon acute starvation

- Dmp53 regulation of Dilp2 levels and autophagy are necessary for starvation survival

CellPress

Article

Fat Body p53 Regulates Systemic Insulin Signaling and Autophagy under Nutrient Stress via *Drosophila* Upd2 Repression

María Clara Ingaramo,[1] Juan Andrés Sánchez,[1] Norbert Perrimon,[3,4,*] and Andrés Dekanty[1,2,5,*]

[1]Instituto de Agrobiotecnología del Litoral, Consejo Nacional de Investigaciones Científicas y Técnicas (CONICET), Santa Fe 3000, Argentina
[2]Facultad de Bioquímica y Ciencias Biológicas, Universidad Nacional del Litoral (UNL), Santa Fe 3000, Argentina
[3]Department of Genetics, Blavatnik Institute, Harvard Medical School, Boston, MA 02115, USA
[4]Howard Hughes Medical Institute, Boston, MA 02115, USA
[5]Lead Contact
*Correspondence: perrimon@genetics.med.harvard.edu (N.P.), adekanty@santafe-conicet.gov.ar (A.D.)
https://doi.org/10.1016/j.celrep.2020.108321

SUMMARY

The tumor suppressor p53 regulates multiple metabolic pathways at the cellular level. However, its role in the context of a whole animal response to metabolic stress is poorly understood. Using *Drosophila*, we show that AMP-activated protein kinase (AMPK)-dependent Dmp53 activation is critical for sensing nutrient stress, maintaining metabolic homeostasis, and extending organismal survival. Under both nutrient deprivation and high-sugar diet, Dmp53 activation in the fat body represses expression of the *Drosophila* Leptin analog, Unpaired-2 (Upd2), which remotely controls Dilp2 secretion in insulin-producing cells. In starved Dmp53-depleted animals, elevated Upd2 expression in adipose cells and activation of Upd2 receptor Domeless in the brain result in sustained Dilp2 circulating levels and impaired autophagy induction at a systemic level, thereby reducing nutrient stress survival. These findings demonstrate an essential role for the AMPK-Dmp53 axis in nutrient stress responses and expand the concept that adipose tissue acts as a sensing organ that orchestrates systemic adaptation to nutrient status.

INTRODUCTION

The ability of an organism to sense nutrient stress and coordinate metabolic and physiological responses is critical for its survival. Over the last years, the p53 tumor suppressor has emerged as an important regulator of cellular metabolism, and its activation has been regularly observed in response to diverse metabolic inputs, such as changes in oxygen levels or nutrient availability (Berkers et al., 2013). It has been shown that p53 interacts with main players in key nutrient-sensing pathways, such as mammalian target of rapamycin (mTOR) and AMP-activated protein kinase (AMPK), leading to modulation of autophagy and lipid and carbohydrate metabolism. p53 restricts tumor development partially by inhibiting glycolysis (Zawacka-Pankau et al., 2011), limiting the pentose phosphate pathway (Jiang et al., 2011), and promoting mitochondrial respiration (Berkers et al., 2013; Liang et al., 2013). Conversely, p53 activation can benefit tumor growth by stimulating adaptive cellular responses in nutrient-deficient conditions. p53 activation is known to induce cell-cycle arrest and promote cell survival in response to transient glucose deprivation (Jones et al., 2005), regulate autophagy and increase cell fitness upon fasting (Scherz-Shouval et al., 2010), and promote cancer cell survival and proliferation after serine or glutamine depletion (Maddocks et al., 2013; Tajan et al.,

2018). Therefore, p53 plays a pivotal role in the ability of cells to sense and respond to nutrient stress, functions that are important not only to control cancer development but also to regulate crucial aspects of animal physiology. Further studies concerning p53 regulation and function in response to nutrient and metabolic challenges at an organismal level would expand our understanding on the role of p53 in normal animal physiology, aging, and disease.

The single *Drosophila* ortholog of mammalian p53 (Dmp53) has also been shown to regulate tissue and metabolic homeostasis (Barrio et al., 2014; Contreras et al., 2018; Ingaramo et al., 2018; Mesquita et al., 2010; Sanchez et al., 2019). Dmp53 regulates energy metabolism through induction of cell-cycle arrest and cell growth inhibition in response to mitochondrial dysfunction (Mandal et al., 2010) by regulating glycolysis and oxidative phosphorylation to promote cell fitness in dMyc-overexpressing cells (de la Cova et al., 2014) and by modulating autophagy protecting the organism from oxidative stress (Robin et al., 2019). Studies in *Drosophila* have also identified tissue-specific roles of Dmp53 in regulating lifespan and adaptive metabolic responses impacting on animal aging and stress survival (Barrio et al., 2014; Bauer et al., 2007; Hasygar and Hietakangas, 2014; Robin et al., 2019), evidencing conserved functions of p53 (Liu et al., 2014, 2017), and positioning *Drosophila* p53

studies as a valuable alternative providing relevant insights on mammalian health and disease.

The insulin pathway is highly conserved from mammals to *Drosophila* and regulates carbohydrate and lipid metabolism, tissue growth, and longevity in similar ways (Taguchi and White, 2008; Wu and Brown, 2006). *Drosophila* insulin-like peptides (Dilps) promote growth and maintain metabolic homeostasis through activation of a unique insulin receptor (dInR) and of a conserved intracellular insulin and insulin-like growth factor (IGF) signaling pathway (IIS) (Andersen et al., 2013; Ikeya et al., 2002). Dietary conditions tightly regulate Dilp2 production and/ or secretion from the insulin-producing cells (IPCs), neuroendocrine cells analogous to pancreatic β-cells located in the fly brain (Ikeya et al., 2002; Rulifson et al., 2002). Interestingly, a nutrient-sensing mechanism in the fat body (FB), a functional analog of vertebrate adipose and hepatic tissues, non-autonomously regulates Dilp2 secretion and couples systemic growth and metabolism with nutrient availability (Géminard et al., 2009). According to the nutritional status, the FB produces signaling molecules capable of promoting or inhibiting insulin secretion from the IPCs (Agrawal et al., 2016; Delanoue et al., 2016; Koyama and Mirth, 2016; Meschi et al., 2019; Rajan and Perrimon, 2012; Sano et al., 2015). Thus, a simple integrated system composed of various organs and conserved signaling pathways regulates metabolic homeostasis and organismal growth in response to nutrient availability.

The FB also functions as the organism's main energy reserve and is responsible for coupling energy expenditure to nutrient status (Arrese and Soulages, 2010). In well-fed animals, circulating insulin activates insulin receptors in the FB and promotes energy storage in the form of glycogen and triacylglycerol (TAG). Upon limited nutrient availability, stored lipids and glycogen are broken down to supply energy for the rest of the body (Arrese and Soulages, 2010). In previous work, we showed that FB-specific inhibition of Dmp53 activity accelerated the consumption of main energy stores, reduced sugar levels, and compromised organismal survival during nutrient deprivation (Barrio et al., 2014). The mechanism by which Dmp53 regulates metabolic homeostasis and organismal survival under nutrient stress is not entirely understood and might involve regulation of specific signaling and metabolic pathways.

Here, we provide evidence that AMPK-dependent Dmp53 activation in the FB non-cell-autonomously regulates TOR signaling and autophagy induction upon acute starvation, which is essential for organismal survival. Dmp53 activation in response to nutritional stress is required for proper communication between the FB and IPCs by modulating the expression of the *Drosophila* Leptin analog, Unpaired-2 (Upd2). Elevated Upd2 levels in adipose cells of starved Dmp53-depleted animals result in sustained Dilp2 circulating levels, activation of insulin/TOR signaling, and impaired autophagy induction in the whole animal, therefore reducing survival rates upon nutrient deprivation. These results indicate that Dmp53 plays an essential role in *Drosophila*, integrating nutrient status with metabolic homeostasis by modulating Dilp2 circulating levels, systemic insulin signaling, and autophagy.

RESULTS

FB Dmp53 Activity Regulates Organismal Resistance to Challenging Nutrient Conditions

To better understand the role of Dmp53 in metabolic homeostasis and nutrient stress response, we sought to analyze the impact of FB-specific inhibition of Dmp53 transcriptional activity on organismal survival upon different nutrient conditions. To specifically reduce Dmp53 activity in the FB, we expressed a dominant-negative version of Dmp53 lacking DNA-binding activity ($Dmp53^{H159.N}$) under the control of the FB *cg-Gal4* driver (referred to as $cg>p53^{H159.N}$). When maintained on a normal diet, $cg>p53^{H159.N}$ larvae exhibited slight change or no difference in pupal size, TAG level, glycogen content, and circulating glucose compared with control flies (Figure S1) (Barrio et al., 2014). Upon starvation, $cg>p53^{H159.N}$ and $cg>p53^{RNAi}$ adult flies exhibited a clear reduction in survival rates accompanied by an accelerated rate of glycogen consumption as reported in previous work (Figures 1A, 1B, and S1) (Barrio et al., 2014). Similarly, 4-h starvation treatment of mid-third instar larvae (mid-L3) led to a rapid decrease in glycogen content in $cg>p53^{H159.N}$ larvae compared with control animals (Figure 1B), indicating that Dmp53 is playing a role in the short-term starvation response both in larval and in adult stages. Consistent with this, Dmp53 is activated upon acute starvation as shown by increased expression of a Dmp53 activity reporter ($p53^{RE}$-GFP, consisting in p53 consensus DNA binding sites driving GFP expression) (Barrio et al., 2014; Lu et al., 2010) following a 4-h starvation treatment (Figure 1C). Interestingly, high-sugar diet (HSD)-fed animals presented higher $p53^{RE}$-GFP levels, which can be blocked by $Dmp53^{H159.N}$ expression (Figure 1D), and $cg>p53^{H159.N}$ larvae showed a strong developmental delay and reduced viability on HSD when compared with control animals (Figures 1E and S1), which suggests a general role of Dmp53 in maintaining metabolic homeostasis under nutrient stress. Together, these results indicate that Dmp53 is activated in FB cells exposed to acute starvation and HSD treatments, and that Dmp53 activation in FB is required for maintaining metabolic homeostasis and promoting survival. Therefore, despite that Dmp53 absence in the FB appears to have minor effects on metabolism under normal diet, it plays a critical role in regulating energetic homeostasis and organismal survival under different nutritional stress conditions.

FB Dmp53 Activity Is Required to Reduce TOR Signaling and Induce Autophagy under Nutrient Deprivation

Because the TOR pathway is a common regulator of energy metabolism, we explored the effects of depleting Dmp53 activity in the FB on TOR pathway activity. We first measured phosphorylation of S6 kinase, a well-described downstream target of TOR activity, by western blot using a phospho-*Drosophila* p70 S6 kinase (Thr398) antibody. Starvation treatment of mid-L3 larvae led to a rapid decrease in TOR-dependent phosphorylation of S6K (p-S6K) in FB extracts (Figure 2A). Expression of $Dmp53^{H159.N}$ under the control of the *cg-Gal4* driver showed higher levels of p-S6K in FB samples of starved animals (Figure 2A). We also analyzed *unk* gene expression, which is induced after TORC1 inhibition (Tiebe et al., 2015), and
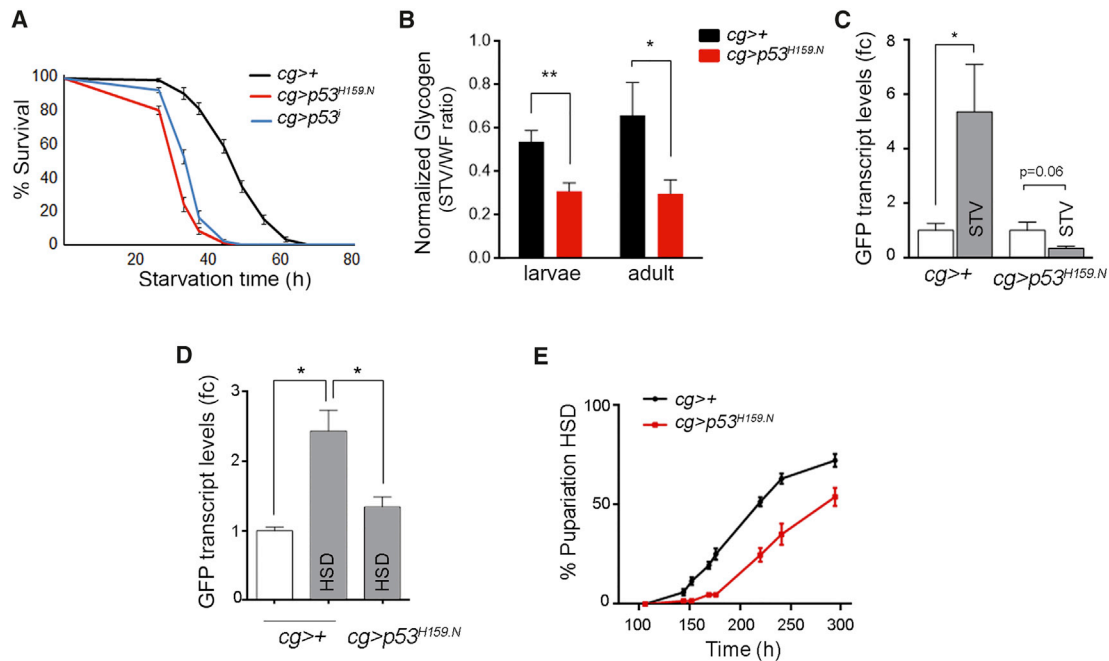
Figure 1. Fat Body Dmp53 Regulates Organismal Response to Challenging Nutrient Conditions

(A) Reduced survival rates to nutrient deprivation of adult flies (males) expressing $Dmp53^{H159.N}$ ($cg>p53^{H159.N}$) or $Dmp53^{RNAi}$ ($cg>p53^i$) under cg-Gal4 control. See Table S1 for n, p, median, and maximum survival values.

(B) Glycogen content in whole larvae and adult flies from the indicated genotypes subjected to starvation (4 h in larvae; 24 h in adults). Data were normalized to protein concentration and presented as a starved (STV)/well-fed (WF) ratio for each genotype.

(C and D) qRT-PCR showing *GFP* mRNA levels in whole larvae (C) and adult flies (D) bearing p53^{RE}-GFP activity reporter and expressing the indicated transgenes under WF, STV, or high-sugar-diet (HSD) conditions. Results are expressed as fold induction with respect to control WF animals. Three independent replicates were carried out for each sample.

(E) Development timing of control ($cg>+$) and $cg>p53^{H159.N}$ animals raised immediately after hatching in HSD.

Mean ± SEM. *p < 0.05; **p < 0.01. See also Figure S1 and Table S1.

observed reduced induction of endogenous *unk* transcript levels in Dmp53-depleted FBs (Figure 2B), strongly suggesting that TOR signaling is maintained more actively in starved Dmp53-depleted animals. To investigate how sustained TORC1 signaling impacts on autophagy induction in starved $cg>p53^{H159.N}$ animals, we used either a transgenic autophagy reporter, mCherry-tagged-Atg8a (mChAtg8), or the cell-permeable LysoTracker dye, which targets acidic organelles, including autolysosomes. A clear accumulation of LysoTracker-positive vesicles was observed in FB cells of wild-type larvae following 4 h of starvation (Figure 2C). Interestingly, starvation-induced autophagy was strongly reduced in *dmp53* mutant animals (*dmp53^ns* and *dmp53^5A14*; Figure 2C) or when expressing Dmp53 dominant-negative versions (Dmp53^H159.N, Dmp53^259.N, and Dmp53^R155H) under *cg*-Gal4 control (Figures 2C–2E). Because *cg-Gal4* is mainly expressed in FB cells, as well as lymph gland and hemocytes, we analyzed autophagy induction upon depletion of Dmp53 activity in the FB by using complementary Gal4 lines. Dmp53^H159.N expression under the control of *lpp*, *ppl*, *R4*, and *Lsp2* Gal4 drivers strongly reduced starvation-induced autophagy (Figures 2E and S2). Similar results were obtained with *cg-Gal4* in combination with *elav-Gal80*, which prevents expression of UAS transgenes in most parts of the brain (Figure S2). In contrast, salivary gland- or

brain-specific depletion of Dmp53 activity (using *SG-Gal4*, *fkh-Gal4*, *elav-Gal4*, and *dilp2-Gal4*) did not have any impact on starvation-induced autophagy (Figure S2). Starvation treatment also showed accumulation of mChAtg8-positive autophagosomes and autolysosomes all through the larval FB that was suppressed in *dmp53^5A14* animals or by Dmp53^H159.N expression (Figures 2F and S2). Note that following long-term starvation (16 h), Dmp53^H159.N-expressing FBs showed accumulation of mChAtg8-positive vesicles, pointing to a defect in short-term starvation response mechanisms (Figure S2). Collectively, these results indicate that Dmp53 activity in the FB regulates TOR activity and autophagy induction upon acute nutrient deprivation.

Next, we asked whether impaired autophagy is responsible for reduced survival rates of $cg>p53^{H159.N}$ animals exposed to starvation. Chloroquine (CQ) inhibits autophagy as it raises lysosomal pH, leading to inhibition of both autophagosome-lysosome fusion and lysosomal protein degradation. Interestingly, whereas CQ treatment renders flies more sensitive to starvation at a similar extent as $cg>p53^{H159.N}$ (Figure 2G), it did not increase sensitivity to starvation of $cg>p53^{H159.N}$ flies. Similar results were obtained when blocking autophagy induction in the FB by expression of ATG1^RNAi (Figure S2), strongly suggesting that inhibition of autophagy contributes to the reduced survival rates of

A

p-S6K

Actin

4h STV

Relative p-S6K/Actin

B

unk transcript levels (fc)

C
4h STV, Lysotracker

D
Relative Lysotracker intensity 4h STV

4h STV, Lysotracker

E

F
mChATG8, *cg-Gal4*
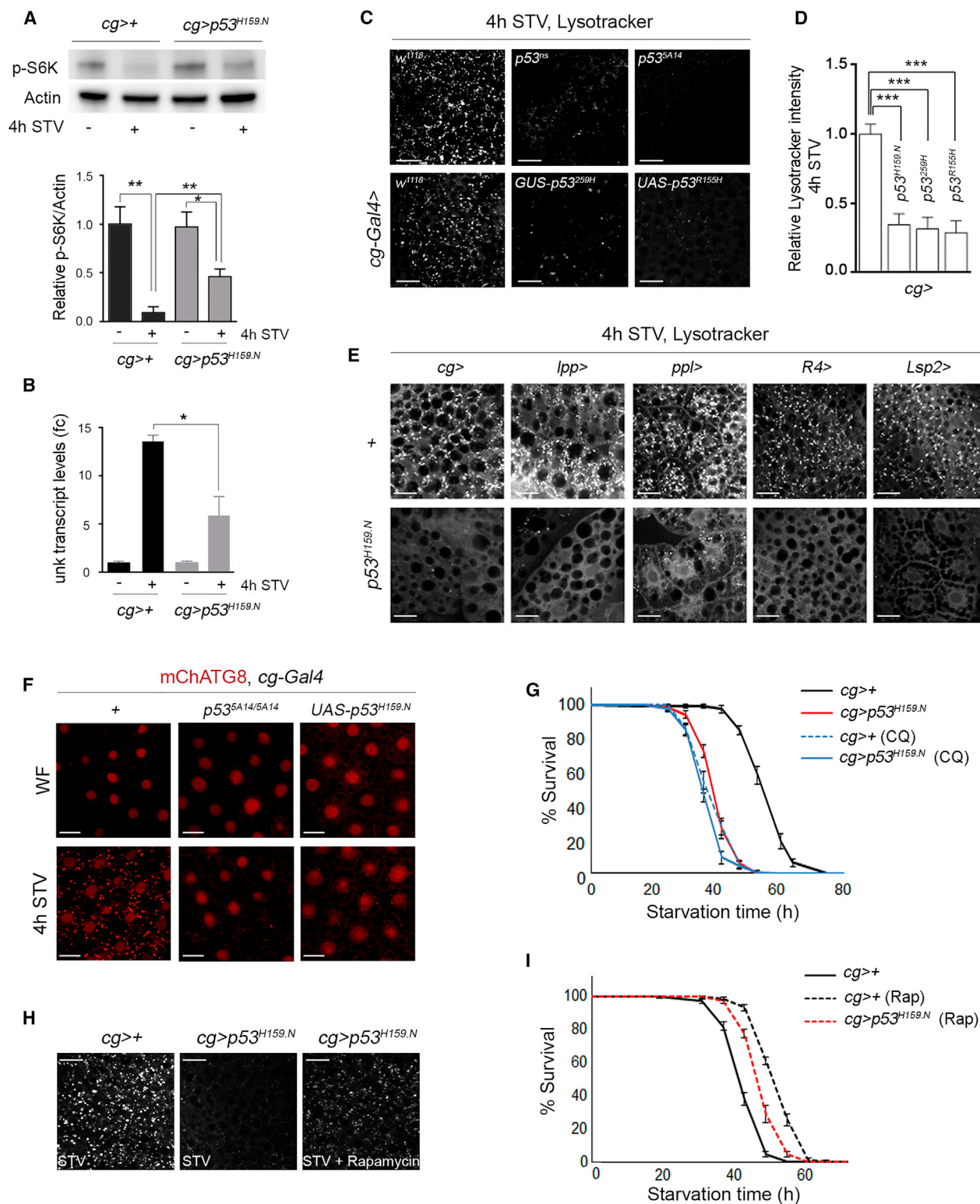
G

H

I

Figure 2. Fat Body Dmp53 Regulates TOR Signaling, Autophagy Induction, and Survival upon Starvation

(A) Immunoblot showing p-S6K levels in FB extracts from control (*cg>+*) and *cg>p53^H159.N* animals in WF and STV conditions. Data were normalized to actin levels and expressed relative to WF animals. Mean ± SEM of three independent experiments are shown.

(legend continued on next page)

starved, Dmp53-depleted animals. We then used rapamycin, a potent inhibitor of TOR signaling, to test whether reducing TOR activity would affect survival rates of Dmp53-depleted animals to starvation. Rapamycin treatment significantly increased starvation resistance of control and $cg>p53^{H159.N}$ adult flies (Figure 2I) and partially rescued autophagy induction (Figures 2H and S2), indicating that sustained TOR activity contributes to the reduced survival rates of starved, Dmp53-depleted animals. Altogether, these data indicate that Dmp53 activation in FB of starved animals is required to reduce TOR signaling, induce autophagy, and promote starvation resistance.

FB Dmp53 Non-Cell-Autonomously Regulates TOR Signaling and Autophagy Induction upon Starvation

Autophagy induction is inhibited by TOR, which is activated both by insulin signaling and directly by nutrients (Rusten et al., 2004; Scott et al., 2004). We then asked whether Dmp53 plays a cell-autonomous or non-autonomous function in regulating starvation-induced autophagy. Notably, expression of Dmp53$^{H159.N}$ in single FB cells by using the actin-flip-out-Gal4 technique was unable to impair autophagy induction following 4-h starvation treatment (Figure 3A; compare mChATG8 accumulation in control [GFP$^-$] and Dmp53$^{H159.N}$ [GFP$^+$]-expressing cells). Next, we analyzed expression of the *unk-lacZ* transcriptional reporter that bears a dimerized enhancer region from *unk* intron 2, which is strongly induced after TORC1 inhibition (Tiebe et al., 2015) (Figure 3C). Upregulation of *unk-lacZ* in the FB of starved animals was significantly reduced when expressing Dmp53$^{H159.N}$ under *cg-Gal4* control (Figure 3C). Interestingly, however, starvation-induced *unk-lacZ* expression was not affected when blocking Dmp53 activity in single FB cells (Figure 3B), strongly suggesting that Dmp53 influences TOR signaling and autophagy induction in a non-cell-autonomous manner. We also analyzed the level of expression of upstream TOR elements, such as TSC2 and Sirtuins, along with several Autophagy-related genes (Atg) and found no significant differences between $cg>p53^{H159.N}$ and controls (Figure S3). To confirm that FB Dmp53 has an impact on systemic autophagy induction, we examined LysoTracker staining in other tissues different from the FB. Interestingly, although we observed a significant increase in LysoTracker-positive puncta in brain, salivary gland, and intestine of starved control animals, autolysosomes were almost completely absent in these tissues upon expression of Dmp53$^{H159.N}$ in the FB (Figure 3D). Altogether, these findings point to a tissue-spe-

cific role of *Drosophila* p53 in regulating systemic TOR signaling and autophagy induction upon fasting.

Dmp53 Activation in the FB Is Required to Reduce Dilp2 Circulating Levels and Systemic Insulin Signaling

As stated before, TOR activity and autophagy induction can be modulated directly by nutrients, as well as by insulin signaling (Scott et al., 2004; Rusten et al., 2004), and the FB integrates nutritional inputs with Dilp2 secretion at the IPCs (Géminard et al., 2009). To study a possible function of FB Dmp53 in controlling systemic insulin signaling, we analyzed Dilp2 protein levels in IPCs upon fasting. As previously described, starvation treatment led to a rapid accumulation of Dilp2 protein in IPCs of control animals (Figure 4A). Expression of Dmp53$^{H159.N}$ in the FB, however, resulted in significantly less Dilp2 accumulation upon acute starvation treatment (Figure 4A). Note that similarly to what is seen with autophagy, following long-term starvation treatment (24 h), $cg>p53^{H159.N}$ animals showed similar Dilp2 protein levels in the IPCs than controls (Figure S4). To confirm IPCs Dilp2 retention, we measured epitope-tagged Dilp2 levels (Dilp2HF) (Park et al., 2014) in hemolymph of starved control and Dmp53-depleted animals by ELISA. Whereas no differences were observed between genotypes in well-fed conditions (Figure S4), elevated levels of circulating insulin were observed in starved $cg>p53^{H159.N}$ animals (Figure 4B). Note that we found no significant difference in *dilp2* and *dilp5* transcript levels between control and Dmp53-depleted larvae in either well-fed or starved conditions (Figure S4).

To assess whether sustained Dilp2 circulating levels in starved Dmp53-depleted animals have an impact on systemic insulin signaling, we first measured *4EBP* and *dInR* transcript levels. These two genes are direct transcriptional targets of dFOXO (Puig et al., 2003; Teleman et al., 2005), which is negatively regulated by the insulin pathway. Consistent with a rapid drop of circulating Dilp2, *4EBP* and *dInR* transcript levels were strongly induced in control larvae upon nutrient deprivation (Figure 4C). Interestingly, however, starvation-induced expression of these genes was significantly reduced in $cg>p53^{H159.N}$ larvae (Figure 4C). Additionally, we used the tGPH reporter for *in vivo* PI3K activity, which consists of a GFP-Pleckstrin Homology domain fusion protein ubiquitously expressed under the control of β-tubulin promoter. tGPH is localized to plasma membrane in FB and salivary gland cells of well-fed animals (Figure S4) (Britton et al., 2002). In contrast, membrane-associated tGPH is diminished under nutrient deprivation as a consequence of reduced

---

(B) qRT-PCR showing *unk* transcript levels in FB samples obtained from *cg>+* and *cg>p53^{H159.N}* larvae in WF or STV conditions. Results are expressed as fold induction with respect to control animals. Three independent replicates were carried out for each sample.

(C) LysoTracker staining to detect autophagy induction in the FB of STV control (*w^{1118}* or *cg>+*), *dmp53* mutant (*p53^{ns}* or *p53^{5A14}*), and Dmp53-depleted (*cg>p53^{259H}* or *cg>p53^{R155H}*) larvae.

(D) Relative LysoTracker intensity of the indicated genotypes. n ≥ 10 for 2 independent experiments.

(E) LysoTracker staining of STV larvae expressing *Dmp53^{H159.N}* in the FB under the control of the indicated Gal4 drivers. In all cases, expression of *Dmp53^{H159.N}* strongly reduced starvation-induced autophagy.

(F) FB cells labeled to visualize autophagic vesicles by using mCherry-Atg8 fusion protein (mChAtg8; in red) in control, *p53^{5A14/5A14}*, and *cg>p53^{H159.N}* animals in WF or STV conditions.

(G and I) Survival rates to nutrient deprivation of adult flies (males) expressing the indicated transgenes under *cg*-Gal4 control and treated with chloroquine (G), rapamycin (I), or the corresponding vehicles. See Table S1 for n, p, median, and maximum survival values.

(H) LysoTracker staining showing that reduced autophagy induction observed in STV *cg>p53^{H159.N}* larvae was partially rescued by rapamycin treatment.

Mean ± SEM. ***p < 0.001; **p < 0.01; *p < 0.05. Scale bars, 25 μm. See also Figure S2 and Table S1.
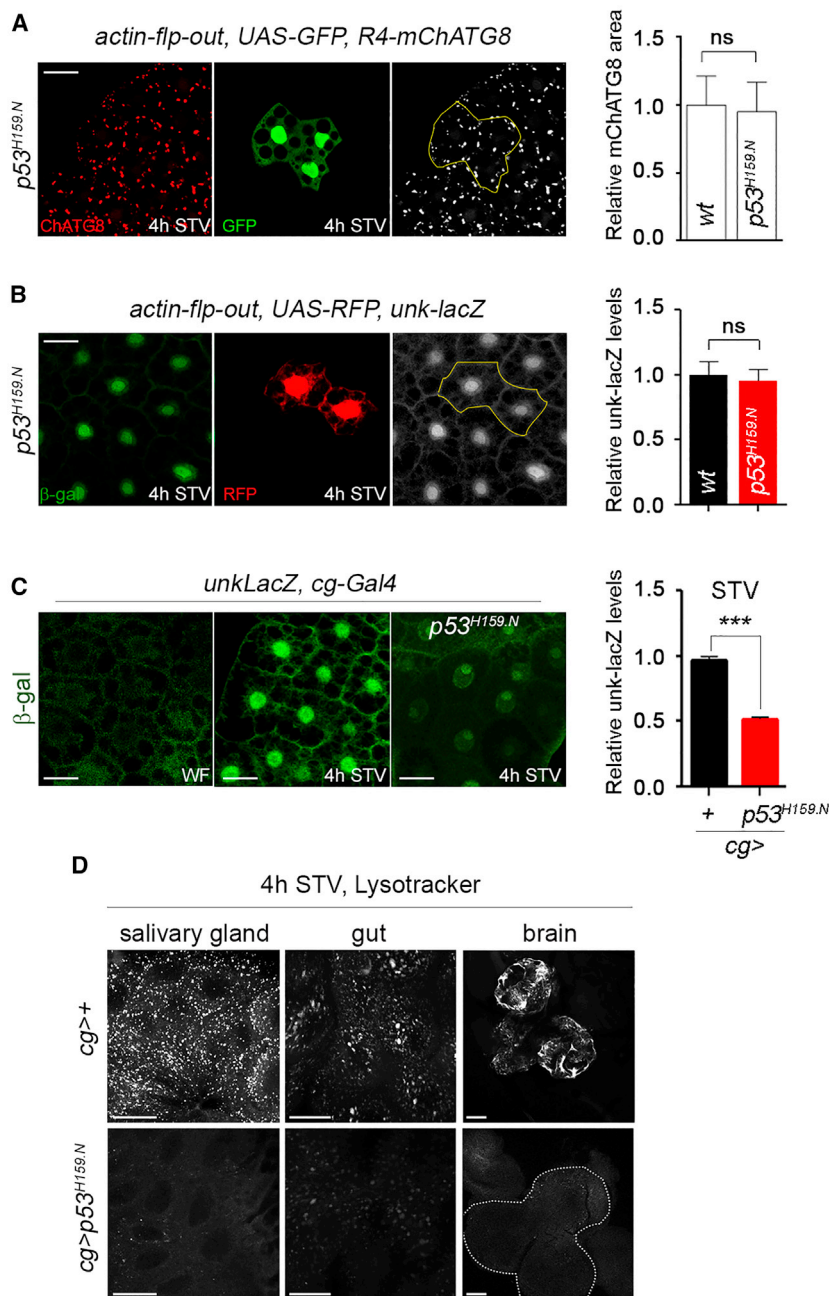
Figure 3. Dmp53 Non-Cell-Autonomously Regulates TOR Signaling and Autophagy upon Starvation

(A) FB cells labeled to visualize mCherry-Atg8 fusion protein (mChAtg8; in red or white). STV FB cells expressing $Dmp53^{H159.N}$ (marked by the expression of GFP, in green) showed similar autophagy induction than neighboring wild-type cells (left). Relative mChAtg8 area (right) between control and $Dmp53^{H159.N}$ expressing cells are shown. n ≥ 10 for 3 independent experiments.

(B) Immunostaining showing *unk-lacZ* expression (β-gal in green or white). STV FB cells expressing $Dmp53^{H159.N}$ (marked by the expression of RFP, in red) showed similar *unk-lacZ* levels than neighboring wild-type cells. Relative *unk-lacZ* levels between control and $Dmp53^{H159.N}$ expressing cells are shown (right). n ≥ 10 for 3 independent experiments.

(C) Immunostaining showing *unk-lacZ* levels (β-gal, green) in the FB of *cg>+* and *cg>p53^{H159.N}* larvae in WF or STV conditions. Relative β-gal fluorescence intensity showing reduced *unk-lacZ* levels in STV *cg>p53^{H159.N}* animals (right). n ≥ 50 for 3 independent experiments.

(D) LysoTracker staining to detect autophagy induction in the salivary gland, intestine, and brain of STV *cg>+* and *cg>p53^{H159.N}* larvae.

Mean ± SEM. ***p < 0.001. Scale bars, 30 μm. ns, not significant. See also Figure S3.

Next, we evaluated to what extent the increased Dilp2 circulating levels observed in starved Dmp53-depleted animals were responsible for their reduced survival rates. Overexpression of ImpL2, a secreted protein that binds Dilp2 and inhibits insulin receptor signaling in a non-cell-autonomous manner, completely reverted the starvation sensitivity caused by Dmp53 activity depletion in the FB (Figure 4F). Additionally, ImpL2 overexpression reverted autophagy induction kinetics in starved *cg>p53^{H159.N}* animals (Figures 4G and S4). Importantly, IPC-specific depletion of Dmp53 activity (using *dilp2-Gal4*) did not have any impact on either starvation sensitivity (Figure S4) or autophagy induction (Figure S2). Taken together, these results indicate that Dmp53 activity in the FB of starved animals reduces Dilp2 circulating levels, therefore influencing systemic insulin and TOR signaling, autophagy induction, and starvation resistance.

Dmp53-Dependent Regulation of Upd2 Influences Dilp2 Levels, Autophagy Induction, and Organismal Survival upon Nutrient Stress

Communication between the FB and the brain relies on humoral signals emitted by fat cells according to nutrient conditions (Britton and Edgar, 1998; Géminard et al., 2009). To further understand the role of Dmp53 in brain-FB intercommunication and the nature of the signals involved, we set up
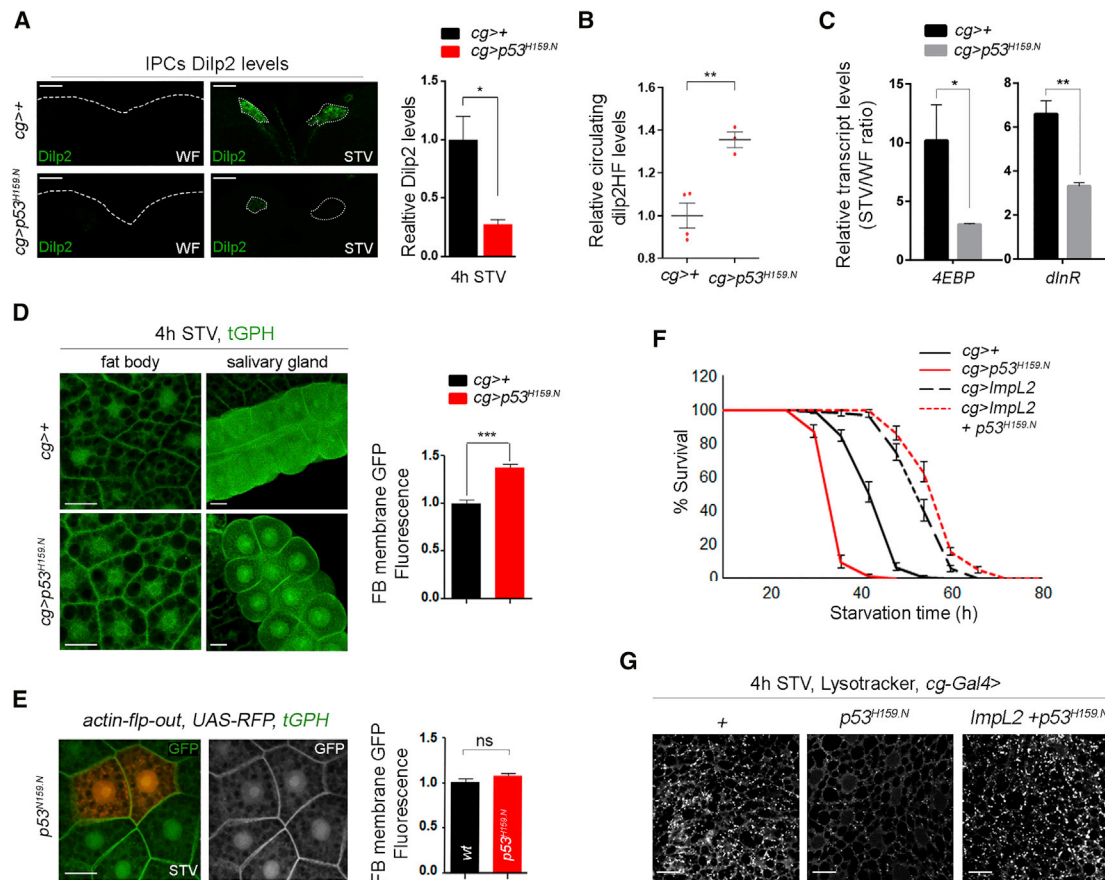
insulin signaling (Figure 4D) (Britton et al., 2002). Impairing Dmp53 transcriptional activity specifically in the FB showed higher tGPH levels at the plasma membrane of starved mid-L3 larvae than control animals (Figure 4D). Consistent with a non-cell-autonomous role of Dmp53 in regulating systemic insulin signaling, these results were observed in cells from both FB and salivary gland (Figure 4D), and expression of Dmp53^{H159.N} in single FB cells did not affect tGPH localization following 4-h starvation treatment (Figure 4E; compare membrane-associated tGPH levels in control [RFP⁻] and Dmp53^{H159.N} [RFP⁺]-expressing cells).

Figure 4. Fat Body Dmp53 Activity Regulates Dilp2 Circulating Levels and Systemic Insulin Signaling

(A) Brain IPCs stained to visualize Dilp2 (green) protein levels in control (*cg>+*) and *cg>p53^H159.N* larvae in WF and STV conditions (left). Relative Dilp2 levels showing reduced accumulation in STV *cg>p53^H159.N* animals (right). n ≥ 10 brains per genotype, representative of 3 independent experiments.

(B) Immunoassays (ELISA) showing increased Dilp2-HF circulating levels in hemolymph of STV *cg>p53^H159.N* compared with *cg>+* animals.

(C) qRT-PCR showing *4EBP* and *dInR* transcript levels in the FB of *cg>+* and *cg>p53^H159.N* animals subjected to WF or STV conditions. Results are expressed as fold induction with respect to WF conditions. Three independent replicates were carried out for each sample.

(D) FB and salivary gland cells labeled to visualize tGPH reporter (green) in *cg>+* and *cg>p53^H159.N* animals in STV. Quantification of relative membrane-GFP fluorescence intensity in the FB (right). n ≥ 40 for 3 independent experiments.

(E) STV FB cells expressing *Dmp53^H159.N* (marked by the expression of RFP, in red) showed similar tGPH levels (in green or white) than neighboring wild-type cells. Relative tGPH levels between control and *Dmp53^H159.N* expressing cells are shown (right). n ≥ 10 for 3 independent experiments.

(F) Survival rates to nutrient deprivation of adult flies (males) expressing the indicated transgenes under *cg*-Gal4 control. ImpL2 overexpression totally reverted the reduced survival rates of *cg>p53^H159.N* flies upon starvation. See Table S1 for n, p, median, and maximum survival values.

(G) LysoTracker staining showing that reduced autophagy induction observed in STV *cg>p53^H159.N* larvae was largely rescued when co-expressing ImpL2.

Mean ± SEM. ***p < 0.001; **p < 0.01; *p < 0.05. Scale bars, 25 μm. See also Figure S4 and Table S1.

ex vivo experiments. Inverted larvae from control (*cg>GFP*) and *cg>p53^N159.H* animals were incubated in M3 insect medium (equivalent to starvation treatment; Kim and Neufeld, 2015) and stained to visualize IPCs Dilp2 levels. Recapitulation of Dilp2 secretion results obtained *in vivo* was evidenced by rapid increase in IPCs Dilp2 levels after 3-h incubation of control inverted larvae in M3 medium compared with inverted larvae at the time of dissection (WF [well-fed], Figure 5A). Inverted larvae from *cg>p53^N159.H* animals showed significantly less Dilp2 accumulation (Figure 5A). Because FB secreted molecules have been described acting either positively or negatively on Dilp2 secretion, we then intended to distinguish between these two possibilities by performing *ex vivo* co-cul-

ture experiments in which inverted larvae from control and *cg>p53^N159.H* animals were incubated together. Interestingly, Dilp2 accumulation levels in the IPCs of control larvae were drastically reduced when co-cultured with *cg>p53^N159.H* inverted larvae (Figure 5A, compare middle and right panels; see also Figure 5B for quantifications of Dilp2 intensity levels). Similar results were obtained when dissected brains from control mid-L3 larvae were cultured in M3 medium in the presence of isolated control or Dmp53-depleted FBs (Figures 5C and 5D). As a physiological readout of insulin/TOR signaling, we also monitored induction of autophagy in *ex vivo* experiments. Whereas *ex vivo* incubation of inverted larvae in M3 medium led to a rapid accumulation of mChATG8-positive
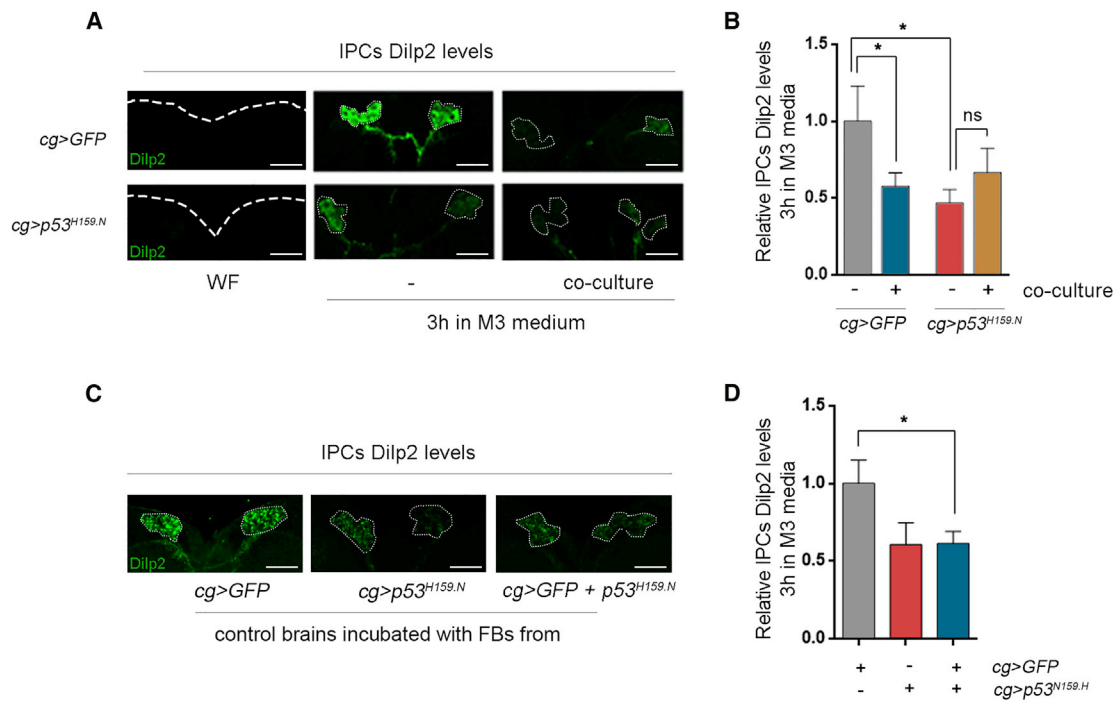
Figure 5. Fat Body Dmp53 Remotely Controls Dilp2 Secretion upon Starvation

Brain IPCs stained to visualize Dilp2 protein levels in *ex vivo* experiments.

(A) Inverted larvae from control (*cg>GFP*) and *cg>p53^H159.N* animals were incubated individually (middle panel) or together (co-culture; right panel) in M3 medium for 3 h and stained to visualize Dilp2 (green) protein levels. Whereas *cg>GFP* or *cg>p53^H159.N* inverted larvae showed high and low Dilp2 accumulation levels when incubated individually, *cg>GFP* animals showed reduced IPCs Dilp2 levels when co-cultured with *cg>p53^H159.N* inverted larvae. Dilp2 protein levels in WF conditions are shown as controls (left panel).

(C) Dissected brains from early L3 larvae were cultured in M3 insect medium in the presence or absence of fat bodies from control (*cg>GFP*) or *cg>p53^H159.N* animals. Whereas control brains incubated *ex vivo* with *cg>GFP* fat bodies showed high Dilp2 accumulation levels, they showed reduced IPCs Dilp2 levels when incubated with fat bodies from *cg>p53^H159.N* animals.

(B and D) Quantification of relative IPCs Dilp2 fluorescence intensity from experiments shown in (A) and (C), respectively. n = 6–8 (B) and n = 5 (D) for 2 independent experiments.

Mean ± SEM. *p < 0.05. Scale bars, 25 μm. ns, not significant. See also Figure S5.

vesicles throughout wild-type larval FB, co-cultures of inverted larvae from wild-type and Dmp53-depleted animals prevented autophagy induction (Figure S5). Altogether, these series of *ex vivo* experiments point to an overproduction of secreted molecules that stimulate Dilp2 secretion by Dmp53-depleted FBs under starvation conditions.

Next, we analyzed the expression of genes encoding FB secreted molecules known to regulate Dilp2 secretion, such as Upd2, CCHa1, CCHa2, GBP1, GBP2, and Sun. qRT-PCR analysis showed significant differences in *upd2* and *sun* transcript levels between controls and *cg>p53^H159.N* larvae exposed to a 4-h starvation treatment (Figure 6A). In contrast, no differences were observed for *ccha1*, *ccha2*, *gbp1*, and *gbp2* mRNA levels (Figure 6A). Thus, we conducted a candidate screen in which these adipokines were specifically silenced in the FB of larvae either well fed or exposed to starvation, and screened for their capacity to recover autophagy induction in *cg>p53^H159.N* animals. Strikingly, *upd2^i* expression in the FB was able to rescue the autophagy delay observed in starved *cg>p53^H159.N* animals (Figures 6B and S6). *Drosophila* cytokine Upd2 has been described as a secreted factor pro-

duced by FB cells in well-fed animals, mainly responding to dietary fat and sugars (Rajan and Perrimon, 2012). FB-derived Upd2 promotes Dilp2 secretion and systemic growth by activating the Janus kinase (JAK)/signal transducer and activator of transcription (STAT) signaling pathway in GABAergic neurons (Rajan and Perrimon, 2012). Notably, depletion of *Drosophila* JAK/STAT receptor Domeless (Dome) in GABAergic neurons by expressing *dome^i* under *vgat-Gal4* control largely reverted impaired autophagy induction observed in starved, *dmp53^5A14* mutant larvae (Figures 6D and S6). Consistent with a role of FB Upd2 in modulating insulin secretion, expressing *upd2^i* along with Dmp53^H159.N showed similar Dilp2 accumulation levels in the IPCs of starved larvae than *upd2^i*-expressing larvae (Figure 6C). We then evaluated at which extent increased Upd2 levels can account for the reduced survival rates observed in starved *cg>p53^H159.N* animals. Notably, *upd2^i* expression fully rescued starvation sensitivity caused by Dmp53 activity depletion in the FB (Figure 6E). Similarly, reduced survival rates displayed by *dmp53^5A14* mutant flies were restored when reducing *Dome* expression in adult GABAergic neurons (Figure 6F). Altogether, our results indicate
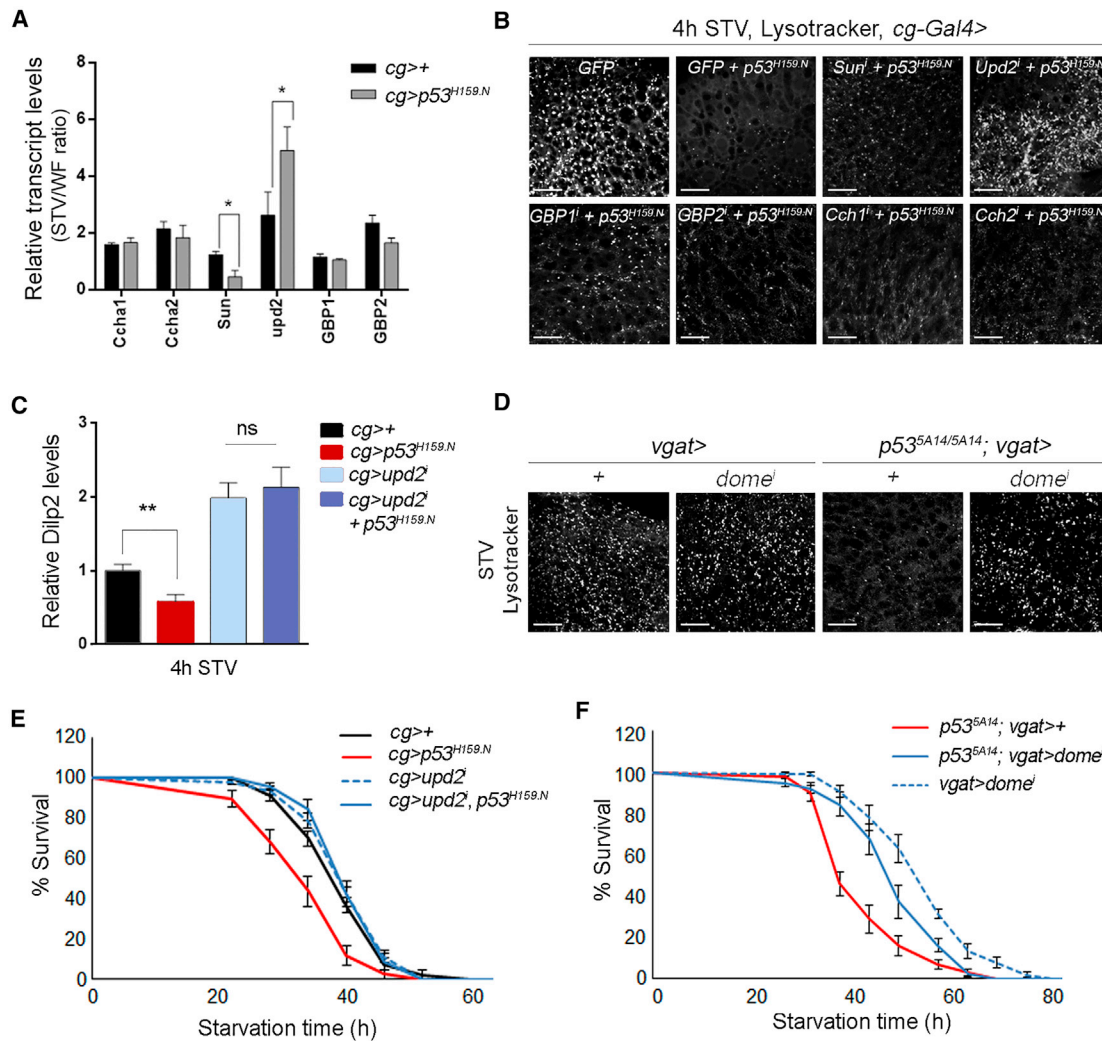
Figure 6. Starvation-Induced Dmp53 Activation Regulates Upd2 Levels, Autophagy Induction, and Survival Rates

(A) qRT-PCR showing mRNA levels of indicated genes in control (*cg>+*) and *cg>p53^H159.N* larvae in WF and STV conditions. Results are expressed as fold induction with respect to WF conditions. Three independent replicates were carried out for each sample.

(B) LysoTracker staining in the FB of STV larvae expressing GFP (control) or *Dmp53^H159.N* along with the indicated transgenes under *cg*-Gal4 control.

(C) Quantification of mean Dilp2 fluorescence intensity in the IPCs of STV larvae expressing the indicated transgenes in the FB under *cg*-Gal4 control. n ≥ 10 brains per genotype, representative of 2 independent experiments.

(D) LysoTracker staining in the FB of STV larvae expressing *dome^i* in GABAergic neurons by using the *vgat*-Gal4 driver in either wild-type or *p53^5A14* mutant background.

(E and F) Survival rates to nutrient deprivation of adult flies (females) expressing the indicated transgenes under the control of *cg*-Gal4 (E) or *vgat*-Gal4 (F) drivers. Inhibiting *Upd2* expression in the FB totally reverted the reduced survival rates of *cg>p53^H159.N* flies upon starvation (E), and blocking JAK/STAT signaling in GABAergic neurons strongly rescued the reduced survival rates of *p53^5A14* mutant flies (F). See Table S1 for n, p, median, and maximum survival values. Mean ± SEM. **p < 0.01; *p < 0.05. Scale bars, 25 μm. ns, not significant. See also Figure S6 and Table S1.

that sustained FB Upd2 expression and activation of JAK/STAT signaling in GABAergic neurons is responsible for increased Dilp2 circulating levels, reduced autophagy induction, and hypersensitivity to starvation displayed by Dmp53-depleted animals. Interestingly, recent chromatin immunoprecipitation sequencing (ChIP-seq) analysis showed Dmp53 binding to Upd2 locus in *Drosophila* embryos and adult heads (Kudron et al., 2018; Kurtz et al., 2019). Considering the identification of a conserved p53 binding site at the same location (Figure S6),

we propose that Dmp53 may directly regulate Upd2 expression in the FB of starved animals.

AMPK-Dependent Dmp53 Activation Regulates Systemic Insulin Signaling and Autophagy Induction upon Nutrient Stress

TOR and AMPKs play essential roles in nutrient sensing and are important regulators of cell growth and metabolism (Grewal, 2009; Hietakangas and Cohen, 2009). Whereas
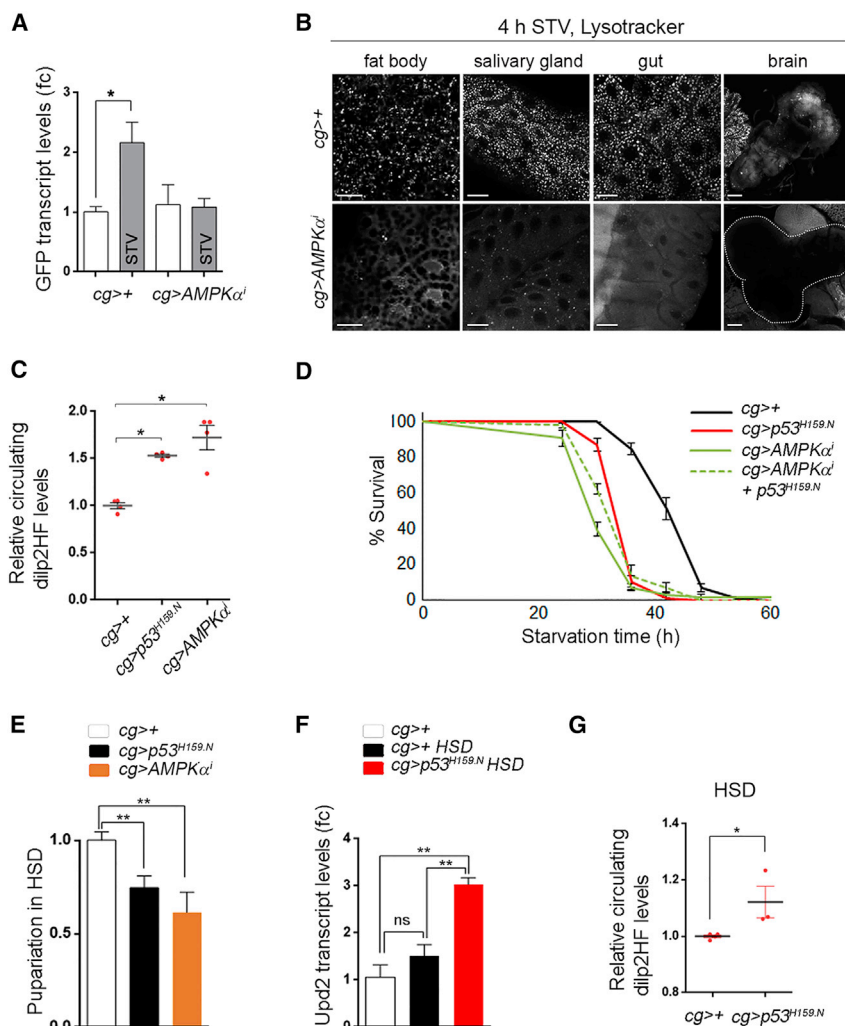
Cell Reports
Article

TOR is regulated in response to amino acid availability, AMPK is modulated by changes in the cellular ATP:AMP ratio. In order to see whether Dmp53 is activated downstream of TOR or AMPK pathways upon acute starvation treatments, we used the Dmp53 activity reporter, *p53^{RE}-GFP*. Although rapamycin treatment of mid-L3 larvae significantly increased *unk* transcript levels, it was not able to increase *p53^{RE}-GFP* expression (Figure S7). In contrast, starvation-induced *p53^{RE}-GFP* was significantly reduced by expression of *AMPKα^i* (Figure 7A). These results prompted us to analyze a possible non-cell-autonomous role of AMPK in controlling autophagy induction upon nutrient deprivation. To determine whether AMPK activity in the FB has an impact on systemic autophagy induction, we examined LysoTracker staining in different tissues of starved animals where AMPK was depleted in the FB by expression of *AMPKα^i* under *cg-Gal4* control (*cg>AMPKα^i*). In all tissues analyzed (brain, salivary gland, intestine, and FB), depletion of FB AMPK levels almost completely blocked autophagy induction when compared with control animals (Figure 7B). Additionally, *AMPKα^i* expres-

sion in single FB cells had no effect on starvation-induced accumulation of mChAtg8 punctae at a cellular level (Figure S7). Next, we measured epitope-tagged Dilp2 levels (Dilp2HF) in the hemolymph of starved control and *cg>AMPKα^i* animals. Starved AMPK-depleted larvae showed higher Dilp2 circulating levels than controls (Figure 7C), suggesting that FB AMPK activity indirectly influences Dilp2 release from IPCs. Even though *AMPK* mutant flies show high starvation sensitivity (Johnson et al., 2010), the contribution of FB AMPK activity on this phenotype has not been addressed so far. Interestingly, the expression of *AMPKα^i* in the FB reduced survival rates of adult flies exposed to starvation conditions at a similar level as *cg>p53$^{H159.N}$* (Figure 7D). Flies expressing *AMPKα^i* along with Dmp53$^{H159.N}$ showed similar survival rates as flies expressing each transgene individually (Figure 7D). Together, these results reveal an AMPK-Dmp53 axis acting in the FB to promote starvation resistance.

Next, we analyzed a possible contribution of FB AMPK-p53 signaling in the response to other nutritional stresses. As shown before, HSD-fed animals showed Dmp53 activation

(Figure 1D), and *cg>p53^H159.N* larvae exhibited reduced viability when compared with control animals (Figures 1E and S1). In addition, *AMPK* knockdown in the FB caused reduced viability of HSD-fed animals (Figure 7E). Notably, *cg>p53^H159.N* animals fed with HSD showed increased *Upd2* expression and elevated Dilp2 circulating levels (Figures 7F and 7G), suggesting that the role of p53 in nutrient sensing and in the regulation of systemic insulin signaling may be a general response to nutrient stress rather than a specific response to starvation. Even though we cannot rule out the possibility of an additive effect of HSD and Dmp53 inhibition on Upd expression, our results suggest that Dmp53 is acting through an endocrine mechanism similar to the one used in starvation.

It has been previously shown that Dilp3, but not Dilp2, is involved in acute responses to altered sugar levels. Dietary sugar stimulates Dilp3 secretion from the IPCs, which in turn promotes systemic TOR activation and suppresses autophagy in the larval FB (Kim and Neufeld, 2015). Interestingly, however, animals reared on a HSD develop insulin resistance and show elevated circulating Dilp2 levels Musselman and Kühnlein, 2018. At which extent, Dilp3 is also playing a role in chronic responses to HSD, and whether altered Dilp3 levels can contribute to Dmp53-dependent phenotypes in excess nutrient stress remain to be studied.

DISCUSSION

A Role of p53 in Organismal Resistance to Challenging Nutrient Conditions

Even though progress has been made in understanding p53 metabolic functions at the cellular level, its role in the context of a whole animal response to metabolic stress is poorly understood. Here, we provide evidence that *Drosophila* p53 is critically involved in nutrient sensing and in the orchestration of an organismal response to nutrient stress. AMPK-dependent Dmp53 activation in the FB in response to nutritional stress is required for proper communication between the FB and the IPCs by modulating the expression of *Drosophila* Leptin analog, Upd2. Elevated Upd2 levels and activation of JAK/STAT signaling in the brain of starved Dmp53-depleted animals result in sustained Dilp2 circulating levels, activation of insulin signaling, and impaired autophagy induction in various tissues, therefore reducing survival rates upon nutrient deprivation. These results position the AMPK-p53 axis as a key player in nutrient sensing and in regulating adaptive physiological responses to low nutrient availability by remotely controlling insulin secretion and autophagy.

Studies in mice have also shown that p53 is activated under several nutrient stress conditions, such as nutrient deprivation, high-caloric diet, and high-fat diet (HFD). p53 becomes activated under nutrient deprivation and regulates expression of genes involved in mitochondrial fatty acid uptake and oxidative phosphorylation (Liu et al., 2014). In turn, pharmacological or genetic inhibition of p53 prevented excessive fat accumulation commonly observed under HFD (Derdak et al., 2013; Yokoyama et al., 2014) and resulted in decreased expression of proinflammatory cytokines and improved insulin

resistance in mice with type 2 diabetes (T2D)-like disease (Minamino et al., 2009). Conversely, upregulation of p53 in adipose tissue caused an inflammatory response that led to insulin resistance (Minamino et al., 2009). These results show that both mice and *Drosophila* p53 activation in individuals exposed to challenging nutrient conditions regulate global metabolism and directly contribute to diet-associated phenotypes.

p53-Dependent Leptin Regulation in Animal Physiology and Disease

Leptin is mainly produced by adipose tissue in mice and humans, and regulates food intake, energy expenditure, and metabolism acting mostly on neuronal targets in the brain. We have shown that Dmp53 activation in the FB under nutrient stress impacts systemic insulin signaling and autophagy induction via regulation of Upd2/Leptin expression. Notably, reduced survival of Dmp53-depleted animals to nutrient deprivation was highly reverted when inhibiting either Upd2 expression in the FB or JAK/STAT signaling in GABAergic neurons in the fly brain. Similar to Upd2, Leptin circulating levels decline during fasting conditions and are increased in animals fed with a HFD (Ahima et al., 1996; Frederich et al., 1995; Rajan and Perrimon, 2012; Rajan et al., 2017). Low Leptin levels during starvation trigger adaptive metabolic and hormonal responses, such as increased appetite and decreased energy expenditure (Ahima et al., 1996; Sano et al., 2015). In HFD-fed mice, p53 activation is necessary for fat accumulation in the liver and adipose tissue, indicating that p53 is essential for coordinating energy expenditure and storage in response to nutrient availability (Liu et al., 2017). Reduced expression of p53 target genes, such as *GLUT4* and *SIRT1*, has been proposed to reduce NAD+ levels and energy expenditure, leading to obesity (Liu et al., 2017). Alternatively, p53 activation in adipose cells could regulate Leptin expression, which is known to act on the CNS to reduce food intake and enhance energy expenditure, thus limiting obesity in times of nutrient abundance. Further investigations into the role of adipose tissue p53 activity in modulating physiological and metabolic responses to stress will be necessary to have a better picture of the role p53 plays in the development of metabolic disorders, such as obesity and T2D. Of importance, based on conserved adipose tissue-specific functions of p53 and signaling pathways involved, studies in *Drosophila* are likely to provide insights relevant to mammalian health and disease.

In the past decade, significant interest has been raised in understanding non-canonical functions of p53 that might have potential roles in tumor suppression (Ingaramo et al., 2018). The fact that p53 is activated in the adipose tissue of obese animals, along with the results here presented concerning a putative direct role of p53 in controlling Upd2/Leptin expression, demonstrates the importance of p53 in regulating metabolism. This is particularly interesting given that epidemiological studies over the last few decades have shown a strong influence of obesity on cancer risk and that increased Leptin can have hormone-like functions affecting tumor development (Andò et al., 2019; Maroni,

2020; Singh et al., 2020; Xu et al., 2020). In this context, our results give insights toward the molecular understanding of p53 activation under metabolic stress and its possible role in tumor suppression acting at either local or organismal level.

Regulation of Adipose p53 Function under Metabolic Stress

TOR and AMPK play essential roles in nutrient sensing, are important regulators of energy balance at both cellular and whole-body levels, and have been shown to interact with p53 (Grewal, 2009; Hietakangas and Cohen, 2009; Jones et al., 2005). We previously showed that TOR inhibition following long starvation treatments (24–48 h) contributes to Dmp53 activation, mainly by alleviating miRNA-mediated targeting of Dmp53 in the FB (Barrio et al., 2014). In this work, we demonstrated that rapid activation of Dmp53 is dependent on AMPK and absolutely required for metabolic and physiological changes that promote organismal resistance to nutrient deprivation. This short-term activation of Dmp53 by AMPK could be part of a dual mechanism along with previously demonstrated long-term activation by lack of TOR, and both of these regulating mechanisms may be important for establishing a rapid response to transient acute nutrient stress also guaranteeing a sustained response when facing a much longer nutrient-deprived period. Given that activated Dmp53 reduces Upd2 expression, systemic insulin, and TOR signaling, it would be reasonable to speculate that Dmp53-dependent TOR inhibition constitutes a positive feedback loop to reinforce Dmp53 activation upon long-term starvation conditions. Therefore, our results place p53 in a crucial position connecting nutrient sensing pathways to endocrine mechanisms, as part of a possible physiological feedback mechanism.

Drosophila AMPK activation has been shown to extend lifespan and promote tissue proteostasis through non-cell-autonomous regulation of autophagy (Stenesen et al., 2013; Ulgherait et al., 2014). Given that Dmp53, acting downstream of AMPK under nutrient stress, non-cell-autonomously regulates Dilp2 levels and autophagy, it will be interesting to determine whether p53, and perhaps its direct phosphorylation by AMPK, is also required for extending organismal lifespan upon tissue-specific AMPK activation.

STAR★METHODS

Detailed methods are provided in the online version of this paper and include the following:

- KEY RESOURCES TABLE
- RESOURCE AVAILABILITY
  - Lead Contact
  - Materials Availability
  - Data and Code Availability
- EXPERIMENTAL MODEL AND SUBJECT DETAILS
- METHOD DETAILS
  - Fly husbandry and mosaic analysis
  - Starvation Treatments, High-Sugar Diet and Survival Experiments
  - Immunostainings

- Western blot
- RNA isolation and quantitative RT-PCR
- Circulating Dilp2 levels in hemolymph
- Fluorescence quantification in IPCs and FB cells
- *Ex vivo* experiments
- Metabolic Assays
- Developmental timing and pupal size
- QUANTIFICATION AND STATISTICAL ANALYSIS

AUTHOR CONTRIBUTIONS

M.C.I. designed and performed experiments, analyzed data, and edited the manuscript. J.A.S. performed experiments. N.P. participated in experimental design and edited the manuscript. A.D. designed experiments, analyzed data, and wrote the manuscript.

REFERENCES

Agrawal, N., Delanoue, R., Mauri, A., Basco, D., Pasco, M., Thorens, B., and Léopold, P. (2016). The Drosophila TNF Eiger Is an Adipokine that Acts on Insulin-Producing Cells to Mediate Nutrient Response. Cell Metab. *23*, 675–684.

Ahima, R.S., Prabakaran, D., Mantzoros, C., Qu, D., Lowell, B., Maratos-Flier, E., and Flier, J.S. (1996). Role of leptin in the neuroendocrine response to fasting. Nature *382*, 250–252.

Andersen, D.S., Colombani, J., and Léopold, P. (2013). Coordination of organ growth: principles and outstanding questions from the world of insects. Trends Cell Biol. *23*, 336–344.

Andò, S., Gelsomino, L., Panza, S., Giordano, C., Bonofiglio, D., Barone, I., and Catalano, S. (2019). Obesity, Leptin and Breast Cancer: Epidemiological Evidence and Proposed Mechanisms. Cancers (Basel) *11*, 62.

Arrese, E.L., and Soulages, J.L. (2010). Insect fat body: energy, metabolism, and regulation. Annu. Rev. Entomol. *55*, 207–225.

Arsham, A.M., and Neufeld, T.P. (2009). A genetic screen in Drosophila reveals novel cytoprotective functions of the autophagy-lysosome pathway. PLoS ONE *4*, e6068.

Barrio, L., Dekanty, A., and Milán, M. (2014). MicroRNA-mediated regulation of Dp53 in the Drosophila fat body contributes to metabolic adaptation to nutrient deprivation. Cell Rep. 8, 528–541.

Bauer, J.H., Chang, C., Morris, S.N.S., Hozier, S., Andersen, S., Waitzman, J.S., and Helfand, S.L. (2007). Expression of dominant-negative Dmp53 in the adult fly brain inhibits insulin signaling. Proc. Natl. Acad. Sci. USA 104, 13355–13360.

Berkers, C.R., Maddocks, O.D.K., Cheung, E.C., Mor, I., and Vousden, K.H. (2013). Metabolic regulation by p53 family members. Cell Metab. 18, 617–633.

Brand, A.H., and Perrimon, N. (1993). Targeted gene expression as a means of altering cell fates and generating dominant phenotypes. Development 118, 401–415.

Britton, J.S., and Edgar, B.A. (1998). Environmental control of the cell cycle in Drosophila: nutrition activates mitotic and endoreplicative cells by distinct mechanisms. Development 125, 2149–2158.

Britton, J.S., Lockwood, W.K., Li, L., Cohen, S.M., and Edgar, B.A. (2002). Drosophila's Insulin/PI3-Kinase Pathway Coordinates Cellular Metabolism with Nutritional Conditions. Dev. Cell 2, 239–249.

Chang, Y.-Y., and Neufeld, T.P. (2009). An Atg1/Atg13 complex with multiple roles in TOR-mediated autophagy regulation. Mol. Biol. Cell 20, 2004–2014.

Contreras, E.G., Sierralta, J., and Glavic, A. (2018). p53 is required for brain growth but is dispensable for resistance to nutrient restriction during Drosophila larval development. PLoS ONE 13, e0194344.

de la Cova, C., Senoo-Matsuda, N., Ziosi, M., Wu, D.C., Bellosta, P., Quinzii, C.M., and Johnston, L.A. (2014). Supercompetitor status of Drosophila Myc cells requires p53 as a fitness sensor to reprogram metabolism and promote viability. Cell Metab. 19, 470–483.

Delanoue, R., Meschi, E., Agrawal, N., Mauri, A., Tsatskis, Y., McNeill, H., and Léopold, P. (2016). Drosophila insulin release is triggered by adipose Stunted ligand to brain Methuselah receptor. Science 353, 1553–1556.

Derdak, Z., Villegas, K.A., Harb, R., Wu, A.M., Sousa, A., and Wands, J.R. (2013). Inhibition of p53 attenuates steatosis and liver injury in a mouse model of non-alcoholic fatty liver disease. J. Hepatol. 58, 785–791.

Frederich, R.C., Hamann, A., Anderson, S., Löllmann, B., Lowell, B.B., and Flier, J.S. (1995). Leptin levels reflect body lipid content in mice: evidence for diet-induced resistance to leptin action. Nat. Med. 1, 1311–1314.

Géminard, C., Rulifson, E.J., and Léopold, P. (2009). Remote control of insulin secretion by fat cells in Drosophila. Cell Metab. 10, 199–207.

Grewal, S.S. (2009). Insulin/TOR signaling in growth and homeostasis: a view from the fly world. Int. J. Biochem. Cell Biol. 41, 1006–1010.

Hasygar, K., and Hietakangas, V. (2014). p53- and ERK7-dependent ribosome surveillance response regulates Drosophila insulin-like peptide secretion. PLoS Genet. 10, e1004764.

Hietakangas, V., and Cohen, S.M. (2009). Regulation of tissue growth through nutrient sensing. Annu. Rev. Genet. 43, 389–410.

Ikeya, T., Galic, M., Belawat, P., Nairz, K., and Hafen, E. (2002). Nutrient-dependent expression of insulin-like peptides from neuroendocrine cells in the CNS contributes to growth regulation in Drosophila. Curr. Biol. 12, 1293–1300.

Ingaramo, M.C., Sánchez, J.A., and Dekanty, A. (2018). Regulation and function of p53: A perspective from Drosophila studies. Mech. Dev. 154, 82–90.

Jiang, P., Du, W., Wang, X., Mancuso, A., Gao, X., Wu, M., and Yang, X. (2011). p53 regulates biosynthesis through direct inactivation of glucose-6-phosphate dehydrogenase. Nat. Cell Biol. 13, 310–316.

Johnson, E.C., Kazgan, N., Bretz, C.A., Forsberg, L.J., Hector, C.E., Worthen, R.J., Onyenwoke, R., and Brenman, J.E. (2010). Altered metabolism and persistent starvation behaviors caused by reduced AMPK function in Drosophila. PLoS ONE 5, e12799.

Jones, R.G., Plas, D.R., Kubek, S., Buzzai, M., Mu, J., Xu, Y., Birnbaum, M.J., and Thompson, C.B. (2005). AMP-activated protein kinase induces a p53-dependent metabolic checkpoint. Mol. Cell 18, 283–293.

Kim, J., and Neufeld, T.P. (2015). Dietary sugar promotes systemic TOR activation in Drosophila through AKH-dependent selective secretion of Dilp3. Nat. Commun. 6, 6846.

Koyama, T., and Mirth, C.K. (2016). Growth-Blocking Peptides As Nutrition-Sensitive Signals for Insulin Secretion and Body Size Regulation. PLoS Biol. 14, e1002392.

Kudron, M.M., Victorsen, A., Gevirtzman, L., Hillier, L.W., Fisher, W.W., Vafeados, D., Kirkey, M., Hammonds, A.S., Gersch, J., Ammouri, H., et al. (2018). The ModERN Resource: Genome-Wide Binding Profiles for Hundreds of Drosophila and Caenorhabditis elegans Transcription Factors. Genetics 208, 937–949.

Kurtz, P., Jones, A.E., Tiwari, B., Link, N., Wylie, A., Tracy, C., Krämer, H., and Abrams, J.M. (2019). Drosophila p53 directs nonapoptotic programs in post-mitotic tissue. Mol. Biol. Cell 30, 1245–1351.

Liang, Y., Liu, J., and Feng, Z. (2013). The regulation of cellular metabolism by tumor suppressor p53. Cell Biosci. 3, 9.

Liu, Y., He, Y., Jin, A., Tikunov, A.P., Zhou, L., Tollini, L.A., Leslie, P., Kim, T.-H., Li, L.O., Coleman, R.A., et al. (2014). Ribosomal protein-Mdm2-p53 pathway coordinates nutrient stress with lipid metabolism by regulating MCD and promoting fatty acid oxidation. Proc. Natl. Acad. Sci. USA 111, E2414–E2422.

Liu, S., Kim, T.H., Franklin, D.A., and Zhang, Y. (2017). Protection against High-Fat-Diet-Induced Obesity in MDM2^{C305F} Mice Due to Reduced p53 Activity and Enhanced Energy Expenditure. Cell Rep. 18, 1005–1018.

Lu, W.-J., Chapo, J., Roig, I., and Abrams, J.M. (2010). Meiotic Recombination Provokes Functional Activation of the p53 Regulatory Network. Science 328, 1278–1281.

Maddocks, O.D.K., Berkers, C.R., Mason, S.M., Zheng, L., Blyth, K., Gottlieb, E., and Vousden, K.H. (2013). Serine starvation induces stress and p53-dependent metabolic remodelling in cancer cells. Nature 493, 542–546.

Mandal, S., Freije, W.A., Guptan, P., and Banerjee, U. (2010). Metabolic control of G1-S transition: cyclin E degradation by p53-induced activation of the ubiquitin-proteasome system. J. Cell Biol. 188, 473–479.

Maroni, P. (2020). Leptin, Adiponectin, and Sam68 in Bone Metastasis from Breast Cancer. Int. J. Mol. Sci. 21, 1051.

Meschi, E., Léopold, P., and Delanoue, R. (2019). An EGF-Responsive Neural Circuit Couples Insulin Secretion with Nutrition in Drosophila. Dev. Cell 48, 76–86.e5.

Mesquita, D., Dekanty, A., and Milán, M. (2010). A dp53-dependent mechanism involved in coordinating tissue growth in Drosophila. PLoS Biol. 8, e1000566.

Minamino, T., Orimo, M., Shimizu, I., Kunieda, T., Yokoyama, M., Ito, T., Nojima, A., Nabetani, A., Oike, Y., Matsubara, H., et al. (2009). A crucial role for adipose tissue p53 in the regulation of insulin resistance. Nat. Med. 15, 1082–1087.

Musselman, L.P., and Kühnlein, R.P. (2018). Drosophila as a model to study obesity and metabolic disease. J. Exp. Biol. 121.

Park, S., Alfa, R.W., Topper, S.M., Kim, G.E.S., Kockel, L., and Kim, S.K. (2014). A genetic strategy to measure circulating Drosophila insulin reveals genes regulating insulin production and secretion. PLoS Genet. 10, e1004555.

Puig, O., Marr, M.T., Ruhf, M.L., and Tjian, R. (2003). Control of cell number by Drosophila FOXO: downstream and feedback regulation of the insulin receptor pathway. Genes Dev. 17, 2006–2020.

Rajan, A., and Perrimon, N. (2012). Drosophila cytokine unpaired 2 regulates physiological homeostasis by remotely controlling insulin secretion. Cell 151, 123–137.

Rajan, A., Housden, B.E., Wirtz-Peitz, F., Holderbaum, L., and Perrimon, N. (2017). A Mechanism Coupling Systemic Energy Sensing to Adipokine Secretion. Dev. Cell 43, 83–98.e6.

Robin, M., Issa, A.R., Santos, C.C., Napoletano, F., Petitgas, C., Chatelain, G., Ruby, M., Walter, L., Birman, S., Domingos, P.M., et al. (2019). Drosophila p53 integrates the antagonism between autophagy and apoptosis in response to stress. Autophagy 15, 771–784.

Rulifson, E.J., Kim, S.K., and Nusse, R. (2002). Ablation of insulin-producing neurons in flies: growth and diabetic phenotypes. Science 296, 1118–1120.

Rusten, T.E., Lindmo, K., Juhász, G., Sass, M., Seglen, P.O., Brech, A., and Stenmark, H. (2004). Programmed autophagy in the Drosophila fat body is induced by ecdysone through regulation of the PI3K pathway. Dev. Cell 7, 179–192.

Sanchez, J.A., Mesquita, D., Ingaramo, M.C., Ariel, F., Milán, M., and Dekanty, A. (2019). Eiger/TNFα-mediated Dilp8 and ROS production coordinate intra-organ growth in Drosophila. PLoS Genet. 15, e1008133.

Sano, H., Nakamura, A., Texada, M.J., Truman, J.W., Ishimoto, H., Kamikouchi, A., Nibu, Y., Kume, K., Ida, T., and Kojima, M. (2015). The Nutrient-Responsive Hormone CCHamide-2 Controls Growth by Regulating Insulin-like Peptides in the Brain of Drosophila melanogaster. PLoS Genet. 11, e1005209.

Scherz-Shouval, R., Weidberg, H., Gonen, C., Wilder, S., Elazar, Z., and Oren, M. (2010). p53-dependent regulation of autophagy protein LC3 supports cancer cell survival under prolonged starvation. Proc. Natl. Acad. Sci. USA 107, 18511–18516.

Schindelin, J., Arganda-Carreras, I., Frise, E., Kaynig, V., Longair, M., Pietzsch, T., Preibisch, S., Rueden, C., Saalfeld, S., Schmid, B., et al. (2012). Fiji: an open-source platform for biological-image analysis. Nat. Methods 9, 676–682.

Scott, R.C., Schuldiner, O., and Neufeld, T.P. (2004). Role and regulation of starvation-induced autophagy in the Drosophila fat body. Dev. Cell 7, 167–178.

Singh, S., Mayengbam, S.S., Chouhan, S., Deshmukh, B., Ramteke, P., Athavale, D., and Bhat, M.K. (2020). Role of TNFα and leptin signaling in colon cancer incidence and tumor growth under obese phenotype. Biochim. Biophys. Acta Mol. Basis Dis. 1866, 165660.

Stenesen, D., Suh, J.M., Seo, J., Yu, K., Lee, K.-S., Kim, J.-S., Min, K.-J., and Graff, J.M. (2013). Adenosine nucleotide biosynthesis and AMPK regulate adult life span and mediate the longevity benefit of caloric restriction in flies. Cell Metab. 17, 101–112.

Taguchi, A., and White, M.F. (2008). Insulin-like signaling, nutrient homeostasis, and life span. Annu. Rev. Physiol. 70, 191–212.

Tajan, M., Hock, A.K., Blagih, J., Robertson, N.A., Labuschagne, C.F., Kruiswijk, F., Humpton, T.J., Adams, P.D., and Vousden, K.H. (2018). A Role for p53 in the Adaptation to Glutamine Starvation through the Expression of SLC1A3. Cell Metab. 28, 721–736.e6.

Teleman, A.A., Chen, Y.-W., and Cohen, S.M. (2005). 4E-BP functions as a metabolic brake used under stress conditions but not during normal growth. Genes Dev. 19, 1844–1848.

Tiebe, M., Lutz, M., De La Garza, A., Buechling, T., Boutros, M., and Teleman, A.A. (2015). REPTOR and REPTOR-BP Regulate Organismal Metabolism and Transcription Downstream of TORC1. Dev. Cell 33, 272–284.

Ulgherait, M., Rana, A., Rera, M., Graniel, J., and Walker, D.W. (2014). AMPK modulates tissue and organismal aging in a non-cell-autonomous manner. Cell Rep. 8, 1767–1780.

Wu, Q., and Brown, M.R. (2006). Signaling and function of insulin-like peptides in insects. Annu. Rev. Entomol. 51, 1–24.

Xu, Y., Tan, M., Tian, X., Zhang, J., Zhang, J., Chen, J., Xu, W., and Sheng, H. (2020). Leptin receptor mediates the proliferation and glucose metabolism of pancreatic cancer cells via AKT pathway activation. Mol. Med. Rep. 21, 945–952.

Yokoyama, M., Okada, S., Nakagomi, A., Moriya, J., Shimizu, I., Nojima, A., Yoshida, Y., Ichimiya, H., Kamimura, N., Kobayashi, Y., et al. (2014). Inhibition of endothelial p53 improves metabolic abnormalities related to dietary obesity. Cell Rep. 7, 1691–1703.

Zawacka-Pankau, J., Grinkevich, V.V., Hünten, S., Nikulenkov, F., Gluch, A., Li, H., Enge, M., Kel, A., and Selivanova, G. (2011). Inhibition of glycolytic enzymes mediated by pharmacologically activated p53: targeting Warburg effect to fight cancer. J. Biol. Chem. 286, 41600–41615.

STAR★METHODS

KEY RESOURCES TABLE

REAGENT or RESOURCE	SOURCE	IDENTIFIER
Antibodies		
Rabbit polyclonal anti-β-galactosidase	Invitrogen	Cat#A11132; RRID: AB_221539
Mouse monoclonal anti-GFP	Developmental Studies Hybridoma Bank	Cat#12A6; RRID: AB_2617417
Rat polyclonal anti-Dilp2	Géminard et al., 2009	N/A
Rabbit anti-phospho-Drosophila S6 Kinase	Cell Signaling	Cat#9209; RRID: AB_2269804
Mouse monoclonal anti-actin	Developmental Studies Hybridoma Bank	JLA20; RRID: AB_528068
Mouse monoclonal anti-FLAG	Sigma	Cat#F1804; RRID: AB_262044
Anti-HA-Peroxidase	Roche	Cat#12013819001; RRID: AB_390917
Chemicals, Peptides, and Recombinant Proteins		
Lysotracker Green	ThermoFisher	Cat#L7526
Rapamycin	LC Labs	Cat#R5000
Critical Commercial Assays		
1-Step Ultra TMB-ELISA Substrate	ThermoFisher	Cat#34029
Amyloglucosidase	Sigma	Cat#A7420
Glucose (GO) Assay Kit	Sigma	Cat#GAGO-20
TRIZOL RNA Isolation Reagent	Invitrogen	Cat#15596026
Halt Protease Inhibitor Cocktail	ThermoFisher	Cat#87785
Cell lysis buffer	Cell Signaling	Cat #9803
SuperSignal West Pico PLUS Chemiluminescent Substrate	ThermoFisher	Cat#34580
Experimental Models: Organisms/Strains		
cg-Gal4	Bloomington Drosophila Stock Center	BDSC:7011
ppl-Gal4	Bloomington Drosophila Stock Center	BDSC:58768
R4-Gal4	Bloomington Drosophila Stock Center	BDSC:33832
lsp2-Gal4	Bloomington Drosophila Stock Center	BDSC:6357
vgat-Gal4	Bloomington Drosophila Stock Center	BDSC:58980
fkh-Gal4	Bloomington Drosophila Stock Center	BDSC:78061
elav-Gal4	Bloomington Drosophila Stock Center	BDSC: 8765
dmp53^{ns}	Bloomington Drosophila Stock Center	BDSC: 23283
dmp53^{5A14}	Bloomington Drosophila Stock Center	BDSC: 6815
UAS-Dmp53^{H159N}	Bloomington Drosophila Stock Center	BDSC: 8420
UAS-Dmp53^{R155H}	Bloomington Drosophila Stock Center	BDSC: 8419
GUS-Dmp53^{259H}	Bloomington Drosophila Stock Center	BDSC: 6582
UAS-Dmp53^{RNAi}	Bloomington Drosophila Stock Center	BDSC: 29351
UAS-AMPKα^{RNAi}	Bloomington Drosophila Stock Center	BDSC: 57785
UAS-sun^{RNAi}	Vienna Drosophila Resource Center	VDRC: 23685
UAS-upd2^{RNAi}	Bloomington Drosophila Stock Center	BDSC: 33949
UAS-ccha1^{RNAi}	Bloomington Drosophila Stock Center	BDSC: 57562
UAS-ccha2^{RNAi}	Bloomington Drosophila Stock Center	BDSC: 57183
UAS-gbp1^{RNAi}	Vienna Drosophila Resource Center	VDRC: 15512
UAS-gbp2^{RNAi}	Vienna Drosophila Resource Center	VDRC: 330018
UAS-dome^{RNAi}	Bloomington Drosophila Stock Center	BDSC: 53890
tGPH	Britton et al., 2002	N/A
unk-lacZ	Tiebe et al., 2015	N/A

Continued

REAGENT or RESOURCE	SOURCE	IDENTIFIER
Dilp2-HF	Park et al., 2014	N/A
p53^{RE}-GFP	Lu et al., 2010	N/A
hsFlp; UAS-Dicer2; R4-Cherry-atg8, act > y+ > Gal4, UAS-GFP	Arsham and Neufeld, 2009	N/A
UAS-mCherry-atg8a	Chang and Neufeld, 2009	N/A
Oligonucleotides		
Oligos used in this study are listed in Table S2		N/A
Software and Algorithms		
Prism	Graph Pad	https://www.graphpad.com/scientific-software/prism/
Adobe Photoshop CS5	Adobe	https://www.adobe.com/uk/products/photoshop.html
Leica Confocal Software	Leica	https://www.leica-microsystems.com/products/microscopesoftware/
Fiji	Schindelin et al., 2012	https://imagej.nih.gov/ij/

RESOURCE AVAILABILITY

Lead Contact
Further information and requests for resources and reagents should be directed to and will be fulfilled by the Lead Contact, Andrés Dekanty (adekanty@santafe-conicet.gov.ar).

Materials Availability
This study did not generate new unique reagents.

Data and Code Availability
Original images and data for figures are available upon request.

EXPERIMENTAL MODEL AND SUBJECT DETAILS

Drosophila melanogaster stocks were reared at 25°C on standard media containing: 4% glucose, 40 g/L powder yeast, 1% agar, 25 g/L wheat flour, 25 g/L cornflour, 4 ml/L propionic acid and 1.1 g/L nipagin. Fly stocks and their resources are listed in the Key Resources Table.

METHOD DETAILS

Fly husbandry and mosaic analysis
Gal4/Upstream Activating Sequence (UAS) binary system was used to drive transgene expression in the different *Drosophila* tissues (Brand and Perrimon, 1993) and experimental crosses were performed at 25°C, unless otherwise specified. Crossing all Gal4 driver lines to w^{1118} background provided controls for each experiment. Flp/Out system was used to generate GFP- or RFP-marked clones. Flies from Flp/Out lines (*hsFLP; act>y+>Gal4, UAS-RFP* or *hsFlp; UAS-Dicer2; R4-Cherry-atg8, act>y+>Gal4, UAS-GFP*) were crossed to corresponding UAS-transgene lines at 25°C and spontaneous recombination events taking place in the fat body prior to the onset of endoreplication were analyzed (Britton et al., 2002).

Starvation Treatments, High-Sugar Diet and Survival Experiments
For starvation treatments in larvae, eggs were collected for 4 h intervals and larvae were transferred to vials containing standard food immediately after eclosion (first instar larvae, L1) at a density of 50 larvae per tube. Larvae were then raised at 25°C for 72h prior to the starvation assay. Mid-third instar larvae were washed with PBS and placed in inverted 60 mm Petri dishes with phosphate-buffered saline (PBS) soaked Whatman paper (starvation, STV) or maintained in standard food (well fed, WF). Each plate was sealed with parafilm and incubated at 25°C for the duration of the experiment. After the starvation period, full larvae or dissected fat bodies were used for immunostaining, RNA/protein extraction or metabolite measurements.

For starvation sensitivity assays, 5- to 7-day-old flies of each genotype were transferred into vials containing 2% agar in PBS. Flies were transferred to new tubes every day, and dead flies were counted every six hours. Control animals were always analyzed in parallel in each experimental condition. Statistics were performed using GraphPad Prism 6.0 software, which uses the Kaplan-Meier estimator to calculate survival fractions as well as median and maximum survival values. Curves were compared using the log-rank (Mantel-Cox) test. The two-tailed p value indicates the value of the difference between the two entire survival distributions at comparison. For chloroquine and rapamycin treatments, adults were transferred to food containing 2.5 mg/ml of chloroquine (Sigma), 400 uM of rapamycin (LC Labs) or an equivalent volume of ethanol as a control. Number of individuals used in each experiment is detailed in Table S1.

For high-sugar diet (HSD) experiments, eggs were collected for 4h interval and larvae were transferred to either standard (4% sucrose) or high-sugar (34% sucrose) food immediately after eclosion (50 L1 larvae per tube). Mid-third instar larvae were used for immunoassay (Dilp2 circulating levels), and 5- to 7-day-old flies were used for RNA extraction. Survival rates were measured as the percent of individuals entering pupariation. At least 120 larvae per genotype were scored. Data were normalized with respect to the control genotype and Student's t test analysis was carried out for statistical significance.

Immunostainings

Mid-third instar larvae were dissected in cold PBS and fixed in 4% formaldehyde/PBS for 20 min at room temperature. Inverted larvae and dissected tissues from *ex vivo* experiments were directly fixed after incubation. They were then washed and permeabilized in PBT (0.2% Triton X-100 in PBS) for 30 min and blocked in BBT (0.3% BSA, 250 mM NaCl in PBT) for 1 h. Samples were incubated overnight at 4°C with primary antibody diluted in BBT, washed three times (15 min each) in BBT and incubated with secondary antibodies for 1.5 hour at room temperature. After three washes with PBT (15 min each), dissected tissues were placed in mounting medium (80% glycerol/PBS containing 0.05% n-Propyl-Gallate). Images were acquired on a Leica SP8 inverted confocal microscope and analyzed and processed using Fiji (Schindelin et al., 2012) and Adobe Photoshop. The following primary antibodies were used: rabbit anti-β-Gal (A11132, Invitrogen); rat anti-Dilp2 (Géminard et al., 2009), mouse anti-GFP (12A6, DSHB). The following secondary antibodies were used: anti-mouse IgG-Alexa Fluor 594; anti-mouse IgG-Alexa Fluor 488; anti-rabbit IgG-Alexa Fluor 594; and anti-rabbit IgG-Alexa Fluor 488 (Jackson InmunoResearch). Antibodies and their resources are listed in the Key Resources Table.

For Lysotracker staining, five mid-third instar larvae either well fed or starved were dissected in cold PBS and incubated 5 min with LysoTracker Green (ThermoFisher) at a final concentration of 0,5 μM in PBS. After washing, dissected tissues were placed in mounting medium (80% glycerol/PBS containing 0.05% n-Propyl-Gallate) and immediately imaged.

Western blot

Dissected fat bodies were homogenized and lysed in 25 μl of cell lysis buffer (Cell Signaling), supplemented with protease inhibitor cocktail (Halt Protease Inhibitor Cocktail, Thermo Fisher Scientific) and protein concentration was determined (Bio-Rad Protein Assay). Twenty-five micrograms of protein extracts were loaded and separated in 4%–20% SDS polyacrylamide gel electrophoresis (Mini-PROTEAN® TGX Precast Protein Gels) and blotted onto PVDF membranes (Immobilion-P, Millipore). Membranes were blocked for 1 hour at room temperature with 5% BSA in TBS-T (TBS with 0.1% Tween 20) and then incubated overnight with mouse anti-actin (DSHB) and rabbit anti-phospho-*Drosophila* S6 Kinase (Cell Signaling) antibodies in TBS-T. Membranes were extensively washed and incubated for 1 hour at room temperature with a peroxidase-conjugated anti-mouse or anti-rabbit secondary antibody (ThermoFisher). Immunoblots were developed with SuperSignal West Pico PLUS Chemiluminescent Substrate (ThermoFisher), imaged with ChemiDoc imager (Bio-Rad) and quantitated using Fiji. Phospho-S6K levels were normalized to actin and represented as fold change respect to control, well fed animals. Data represent mean ± SEM of three independent experiments.

RNA isolation and quantitative RT-PCR

To measure mRNA levels, total RNA was extracted from adults, whole larvae, or dissected FBs of 30 animals using TRIZOL RNA Isolation Reagent (Invitrogen). First strand cDNA synthesis was performed using an oligo(dT)18 primer and RevertAid reverse transcriptase (ThermoFisher) under standard conditions. Quantitative PCR was performed on an aliquot of the cDNA with specific primers using the StepOnePlus Real-Time PCR System. Expression values were normalized to *actin* transcript levels. Data were then normalized to control WF animals using the ΔΔ-CT and fold change was calculated afterward. In all cases, three independent samples were collected from each condition and genotype. Student's t test was used for statistical analysis.

Circulating Dilp2 levels in hemolymph

Dilp2 circulating levels in the hemolymph of well-fed or starved animals were quantified by sandwich ELISA as previously described (Park et al., 2014). Hemolymph was obtained by bleeding washed larvae on ice, and collected in tubes with 55 μL cold PBS. Supernatant after centrifugation at 1,000 x g for one minute was used for ELISA. Briefly, coated plates (Greiner 655061) were incubated overnight at 4°C with monoclonal anti-FLAG antibody (2.5 μg/ml, Sigma F1804) diluted in 0.2M sodium carbonate/bicarbonate buffer, pH 9.4. Plates were washed with PBTw (0,2% Tween-20 in PBS) and blocked with PBS containing 2% BSA overnight at 4°C. Plates were then washed with PBTw before adding hemolymph. Samples were mixed with anti-HA-Peroxidase (Roche #12013819001) at a dilution of 1:350 in PBS-Tween-20 2%, added to plates and incubated overnight at 4°C. Plates were extensively washed with PBTw

and incubated with 1-Step Ultra TMB-ELISA Substrate (ThermoFisher #34029) for 25 min at RT. The reaction was stopped by adding 2M sulfuric acid and absorbance was measured immediately at 450nm.

Fluorescence quantification in IPCs and FB cells

For fluorescence quantification, confocal Z series were taken using a Leica SP8 confocal microscope as described below and identical microscope settings and all subsequent treatments of images were used for control and experimental samples. Total fluorescence intensity of maximum Z-projections was measured using Fiji and data were normalized to control animals. Student's t test analysis was carried out for statistical significance. To quantify Dilp2 intensity levels in larval brains, confocal sections covering the entire IPCs were obtained. To quantify β-gal (*unk-lacZ* reporter) intensity levels in FB cells, confocal sections covering the entire nuclei were taken from 10 FBs and nuclei fluorescence were assessed. To quantify membrane GFP (tGPH reporter) intensity levels, confocal sections covering a 5 micron plasma membrane section were taken from 10 FBs. To quantify Lysotracker intensity levels and mCherry-ATG8 positive punctae, randomly selected pictures were loaded in FIJI and automatically processed. Total fluorescence intensity (Lysotracker) and area (mCh-ATG8) were scored and normalized to control animals. At least 10 images taken from 6-8 animals, and 2-3 independent experiments, per genotype and condition were analyzed. Student's t test was used for statistical analysis.

Ex vivo experiments

For *ex vivo* incubation experiments of whole inverted larvae (carcasses containing fat body, brain and other tissues) sixteen mid-third instar larvae per condition were used. After washing and disection, inverted larvae were incubated in 50 μL of Shields and Sang M3 Insect Medium (Sigma) at room temperature for 3 h. Incubation of inverted larvae in M3 medium has been previously shown to reduce TOR pathway activity and induce autophagy resembling starvation (Kim and Neufeld, 2015). Inverted animals were then fixed, permeabilized, and inmunostained as described above using rat anti-Dilp2 antibodies (1/400). In the case of co-culture experiments, eight inverted larvae from each genotype (cg>GFP and cg>p53[H159.N]) were incubated together in M3 medium and all subsequent steps were performed in the same tube to minimize variability. Dissected brains from 6-8 larvae per genotype and condition were imaged and used for quantification.

For *ex vivo* incubation experiments of dissected tissues, brains from eight wild-type mid-third instar larvae were co-incubated with eight dissected fat bodies from the different genotypes (cg>GFP and cg>p53[H159.N]) in 25 μL of M3 medium at room temperature for 3 h. After immunostaining with anti-Dilp2 antibodies, five brains were placed in mounting medium, imaged, and Dilp2 fluorescence quantified.

Metabolic Assays

TAG, glycogen and glucose levels were determined as previously described (Barrio et al., 2014). Briefly, mid-third instar larvae or 5-7 days old adult flies were fast frozen in liquid nitrogen, homogenized in 200 μl of PBS and immediately incubated at 70°C for 10 min to inactivate endogenous enzymes. For quantification of glucose, hemolymph from 15 larvae was diluted 1:100 and incubated at 70°C for 5 min. TAG levels were determine using a serum triglyceride determination kit (Sigma, TR0100) according to the manufacturer's protocol. For glycogen measurements, 40 μl of heat-treated homogenates were incubated with or without 1 unit of Amyloglucosidase (Sigma, A7420) for 2 hr at 55°C and assayed using a Glucose (GO) Assay Kit (Sigma, GAGO-20). Glycogen amounts were determined by subtracting from the total amount of glucose present in the sample treated with amiloglucosidase the amount of free glucose of untreated samples. Metabolite levels were normalized to protein concentration (BioRad Protein Assay). Five replicates for each genotype and condition were performed, and data were represented as a percentage of the corresponding levels in fed condition for each genotype.

Developmental timing and pupal size

For developmental timing, eggs were collected for 4h interval and first instar larvae were transferred to new vials containing either standard (4% sucrose) or high-sugar (34% sucrose) food immediately after eclosion at a density of 50 larvae per tube. Larvae were then raised at 25°C and the number of pupae was counted at different time points. Five replicates for each genotype and condition were performed, and the resulting percentage of pupae was calculated.

For pupal size measurements, volume was calculated by the formula $4/3\pi(L/2)(l/2)2$ (L, length; l, diameter). Images were taken with a Leica MZ10F Stereoscope, and measures were done using ImageJ software. Pupal size values were shown as the ratio with respect to control animals.

QUANTIFICATION AND STATISTICAL ANALYSIS

For starvation sensitivity assays statistics were performed using GraphPad Prism6, which uses the Kaplan-Meier estimator to calculate survival fractions as well as median and maximum survival values. Curves were compared using the log-rank (Mantel-Cox) test. The two-tailed p value indicates the value of the difference between the two entire survival distributions at comparison.

Graphpad Prism6 was used for statistical analysis and graphical representations based on three or more replicates for each experiment. All significance tests were carried out with unpaired two tailed Student's t tests. Significance P values: $*p < 0.05$, $**p < 0.01$, $***p < 0.001$, $****p < 0.0001$, $^{ns}p > 0.05$.

Images were acquired on a Leica SP8 inverted confocal microscope and analyzed and processed using Fiji (Schindelin et al., 2012) and Adobe Photoshop. Tissue orientation and/or position was adjusted in the field of view for images presented. No relevant information was affected. The original images are available upon request.
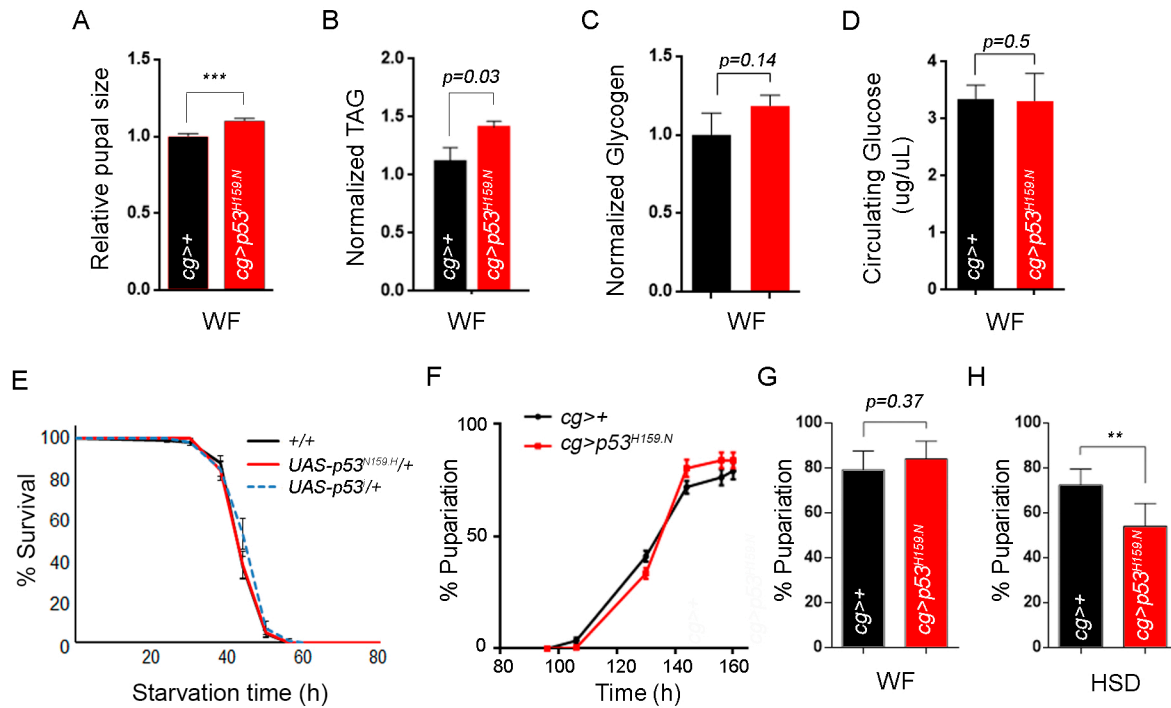
Supplemental Information

Fat Body p53 Regulates Systemic Insulin Signaling

and Autophagy under Nutrient Stress

via *Drosophila* Upd2 Repression

María Clara Ingaramo, Juan Andrés Sánchez, Norbert Perrimon, and Andrés Dekanty

Figure S1. Related to Figure 1.

(A-D) Relative pupal size (A), TAG (B), glycogen (C) and circulating glucose (D) levels of control (*cg>+*) and *cg>p53^{H159.N}* larvae maintained in standard food (well-fed conditions; WF). (E) Survival rates to nutrient deprivation of parental adult flies (males) from the indicated genotypes. See Table S1 for n, p, median, and maximum survival values. (F) Development timing of control and *cg>p53^{H159.N}* animals raised in standard food. (G-H) Percentage of individuals entering pupariation from control and *cg>p53^{H159.N}* animals raised immediately after hatching in WF (G) or HSD (H). Mean ± SEM. * p<0.05; ** p<0.01: ***p>0.001.

Figure S2. Related to Figure 2.
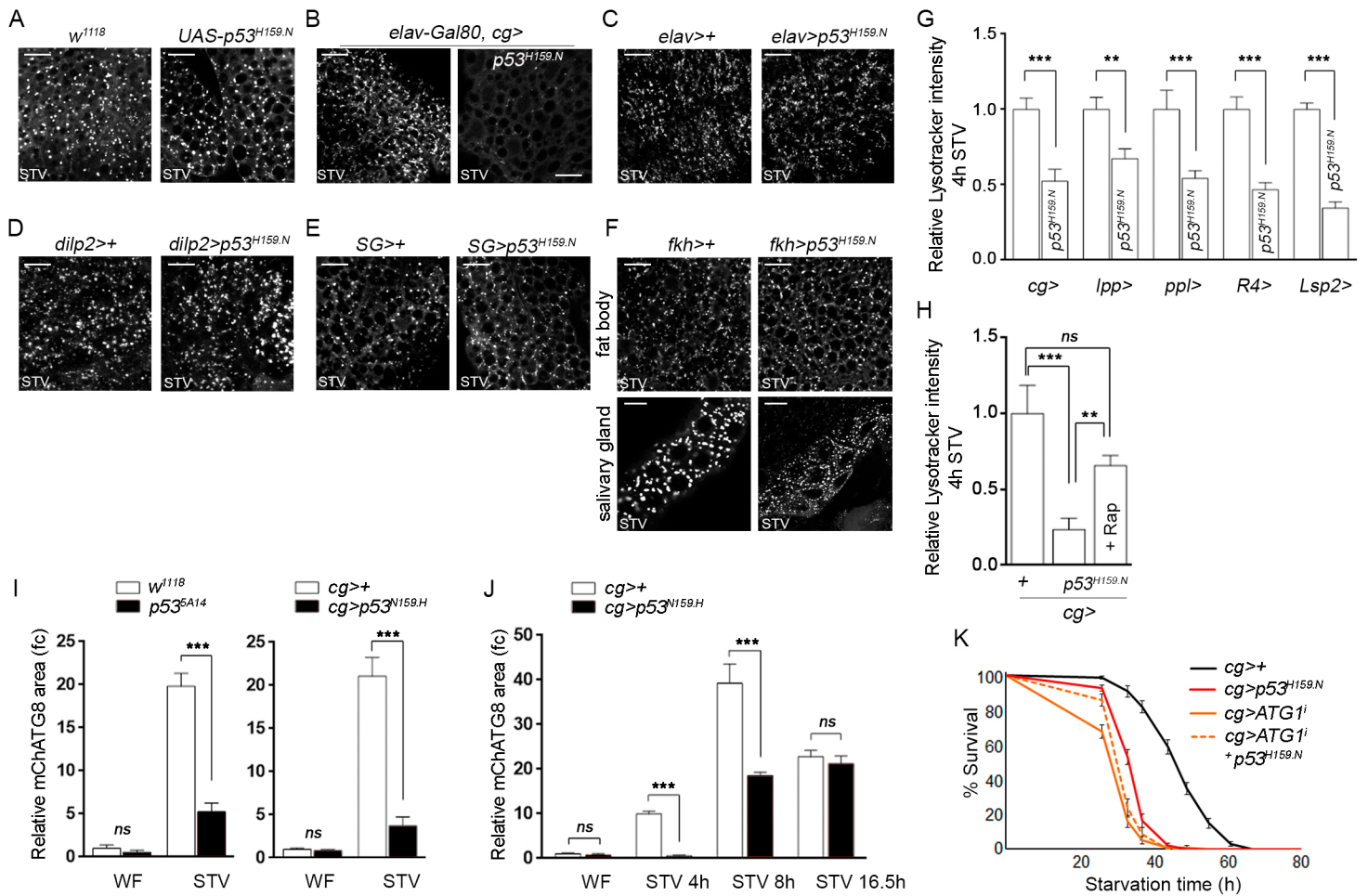
(A) Lysotracker staining showing autophagy levels in the FB of starved larvae from control parental lines: w^{1118} and *UAS-Dmp53$^{H159.N}$*. (B-F) Lysotracker staining showing autophagy levels in the FB (B-F) or salivary gland (F, bottom panel) of starved larvae expressing Dmp53$^{H159.N}$ in different tissues under the control of the indicated Gal4 drivers. *SG-* and *Fkh-Gal4* drives expression to the salivary glands; *dilp2-Gal4* drives expression to the IPCs; *elav-Gal4* drives expression to the nervous system; the combination *elav-Gal80, cg-Gal4* drives expression to the FB while blocking any missexpression in the brain. (G) Relative lysotracker intensity of the indicated genotypes showing significantly reduced autophagy induction when depleting Dmp53 activity in the FB of STV animals; related to Fig. 2E. n≥10 for 2 independent experiments (H) Relative lysotracker intensity showing that reduced autophagy induction observed in starved *cg>p53$^{H159.N}$* larvae was partially rescued by Rapamycin treatment; related to Fig. 2H. n= 5-10 for 2 independent experiments. (I) Relative mChATG8 area of the indicated genotypes showing significantly reduced autophagy induction in starved *dmp53^{5A14}* and *cg>p53$^{H159.N}$* fat bodies; related to Fig. 2F. n≥10 for 2 independent experiments. (J) Time course analysis of starvation-induced autophagy (0-16h, PBS) in the FB of control (*cg-Gal4,UAS-mChAtg8/+*) and Dmp53-depleted (*cg-Gal4,UAS-mChAtg8/UAS-Dmp53$^{H159.N}$*) larvae. n≥10 for 2 independent experiments. (K) Survival rates to nutrient deprivation of adult flies (males) expressing the indicated transgenes in the FB under the control of *cg-Gal4 driver*. *Cg>ATG1^i* animals exhibited greater reduction of survival rates than *cg>p53$^{H159.N}$*. Flies expressing ATG1[RNAi] along with Dmp53$^{H159.N}$ showed similar survival rates as flies expressing ATG1[RNAi]. See Table S1 for n, p, median, and maximum survival values.

Mean ± SEM. ***p<0.001; **p<0.01; *p<0.05. Scale bars, 25 μm.

Figure S3. Related to Figure 3.

A

B
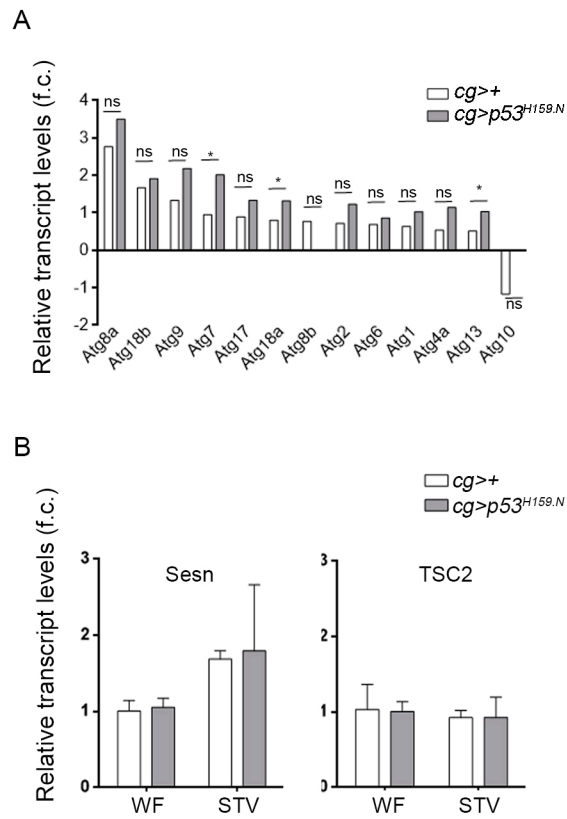
(A-B) Relative transcript levels of *Autophagy-related genes* (*Atg*), *TSC2* and *sestrin* (*sesn*) in FB samples obtained from control (*cg>+*) and *cg>p53^{H159.N}* larvae in WF or STV conditions. Results are expressed as fold induction respect to control animals in WF condition. Mean ± SEM. *p<0.05; ns: not significant.

Figure S4. Related to Figure 4.
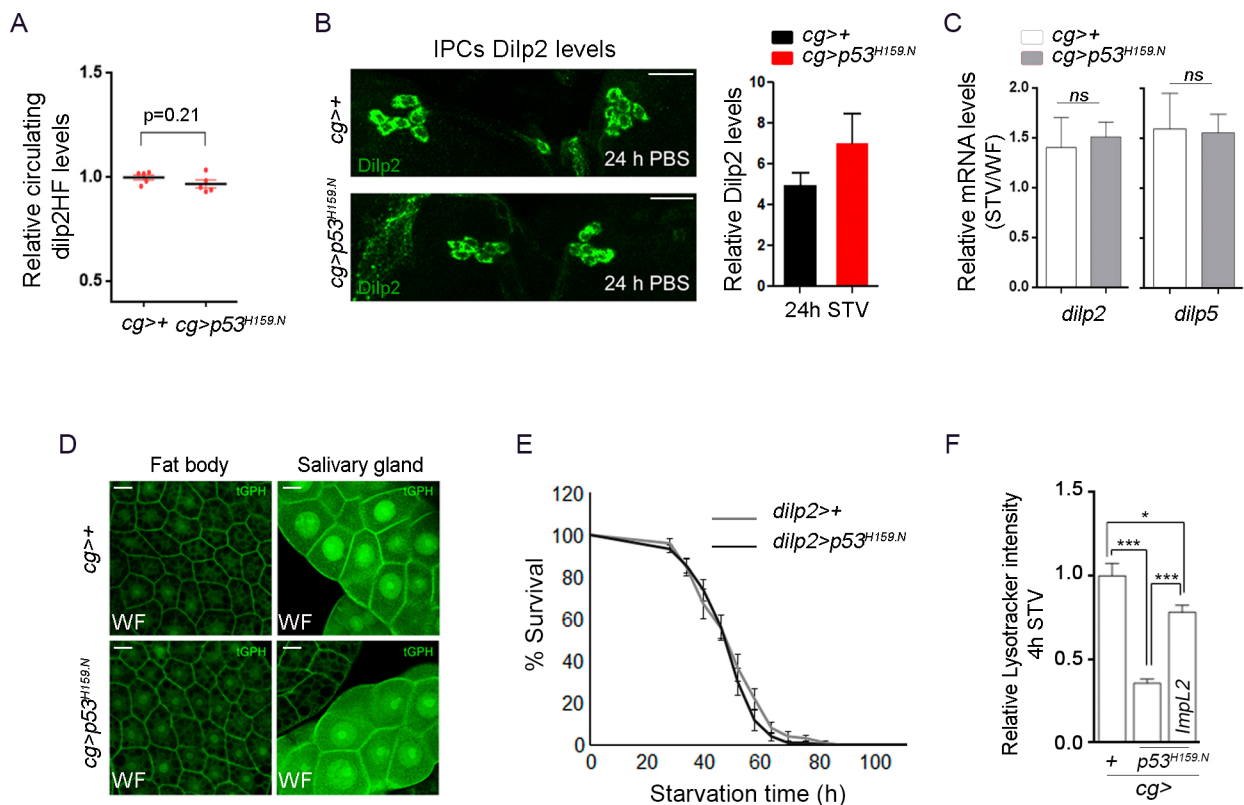
(A) Immunoassays (ELISA) showing Dilp2-HF circulating levels in hemolymph of WF animals. No significant differences were observed in *cg>p53^H159.N* compared to control (*cg>+*). (B) Brain IPCs stained to visualize Dilp2 (green) protein levels in 24 h starved control (*cg>+*) and *cg>p53^H159.N* larvae (left). Mean Dilp2 fluorescence intensity (right) were normalized to control flies upon 4h STV. n≥ 10 brains per genotype, representative of three independent experiments. (C) qRT-PCR showing *dilp2* and *dilp5* transcript levels in samples obtained from control (*cg>+*) and *cg>p53^H159.N* larvae in WF or STV conditions. No significant differences were observed between genotypes. Results are expressed as fold induction respect to control animals. Three independent replicates were carried out for each sample. (D) FB and salivary gland cells labelled to visualize tGPH reporter (green) in control (*cg>+*) and Dmp53-depleted animals (*cg>p53^H159.N*) in WF conditions. (E) Survival rates to nutrient deprivation of adult flies (males) expressing *Dmp53^RNAi* in the IPCs under *dilp2-Gal4* control (*dilp2>p53^N159.H*). See Table S1 for n, p, median, and maximum survival values. (F) Relative lysotracker intensity showing that reduced autophagy induction observed in starved *cg>p53^H159.N* larvae was rescued by ImpL2 overexpression; related to Fig. 4G. n≥10 for 2 independent experiments.
Mean ± SEM. *p<0.05; ***p>0.001; ns: not significant. Scale bars, 25 μm.

Figure S5. Related to Figure 5.

mChATG8

cg>GFP

–   incubated with
                     cg>p53^DN
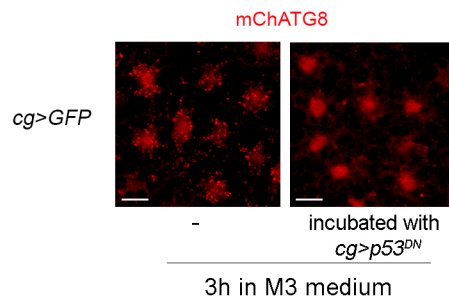
3h in M3 medium

Fat bodies from control (*cg>GFP*) larvae stained to visualize autophagy levels (mChAtg8, red) in *ex vivo* experiments. Note that whereas *ex vivo* incubation of *cg>GFP* inverted larvae in M3 medium led to a rapid accumulation of mChATG8 positive vesicles throughout the FB, co-cultures of control and *cg>p53^N159.H* inverted larvae prevented autophagy induction. Scale bars, 25 μm.

Figure S6. Related to Figure 6.
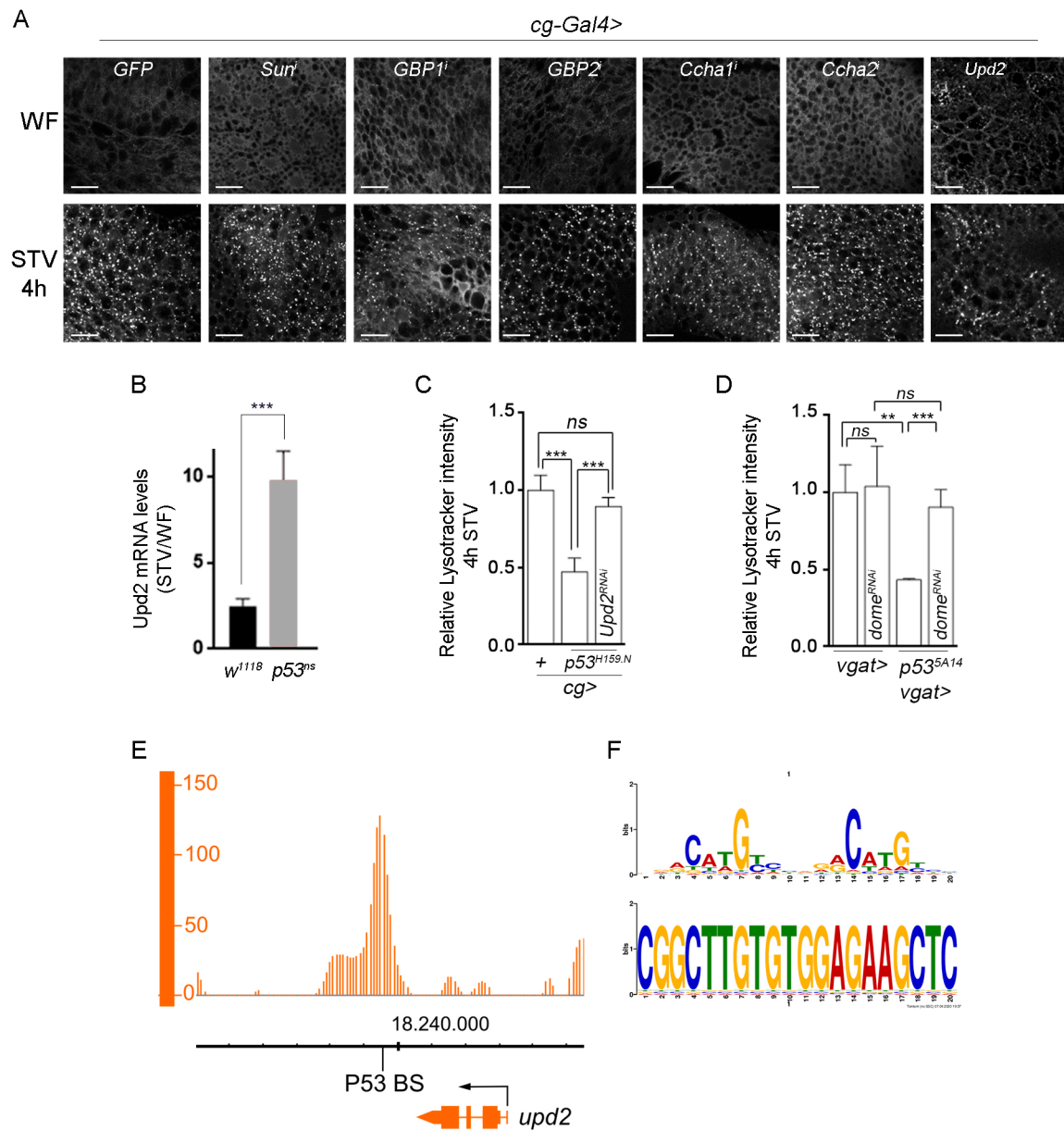
(A) Lysotracker staining showing autophagy levels in the FB of WF or STV (4h PBS) larvae expressing the indicated transgenes under *cg-Gal4* control. (B) qRT-PCR showing *upd2* transcript levels in samples obtained from control (*w^1118^*) and *dmp53* mutant (*dmp53^NS^*) larvae in WF or STV conditions. Results are expressed as fold induction respect to WF conditions for each genotype. Three independent replicates were carried out for each sample. (C) Relative lysotracker intensity showing that reduced autophagy induction observed in starved *cg>p53^H159.N^* larvae was rescued by *Upd2^RNAi^* expression; related to Fig. 6B. n≥10 for 2 independent experiments. (D) Relative lysotracker intensity of the indicated genotypes showing that blocking JAK/STAT signaling in GABAergic neurons strongly rescued the reduced autophagy induction observed in starved *dmp53^5A14^* mutant larvae; related to Fig. 6D. n≥10 for 2 independent experiments.
(E) Histogram showing Dmp53 binding to Upd2 genomic region based on public ChIP-seq data Project ModERN (Kudron 2018) using IGB visualizer (Freese 2016). (F) Consensus (top) and putative (bottom) p53 binding site in Upd2 genomic region.
Mean ± SEM. **p<0.01; ***p>0.001; ns: not significant. Scale bars, 25 μm.

Figure S7. Related to Figure 7.
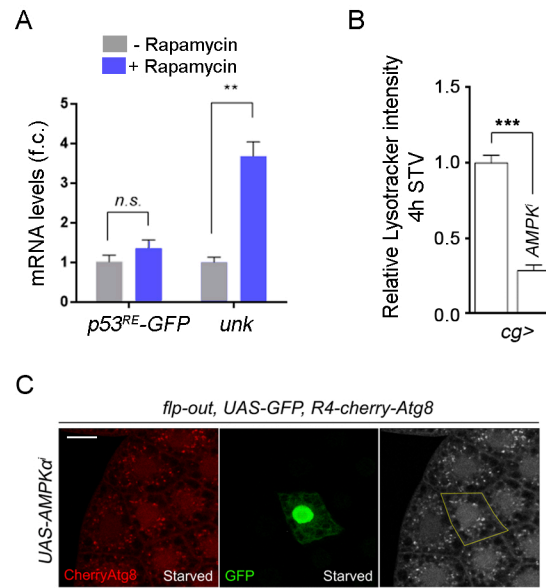
(A) qRT-PCR showing *gfp* or *unk* transcript levels in the FB of wild type larvae after 4h Rapamycin or vehicle treatment. Results are expressed as fold induction with respect to control animals in fed conditions. Three independent replicates were carried out for each sample. (B) Relative lysotracker intensity of the indicated genotypes showing significantly reduced autophagy induction when depleting AMPK in the FB of STV animals; related to Fig. 7B. n≥10 for 2 independent experiments. (C) FB cells labelled to visualize autophagic vesicles by using mCherry-Atg8 fusion protein (mChAtg8; in red or white). Starved FB cells expressing *AMPK^i* (marked by the expression of GFP, in green) showed similar autophagy induction than neighboring wild-type cells.

Mean ± SEM. **p<0.01; ***p>0.001; ns: not significant. Scale bars, 25 μm.

Table S1. Related to Figures 1, 2, 4, 6, 7, S1, S2 and S4

Table compiling the number of individuals (n), p-values according to the Mantel-cox test, median and maximun survival values (h) corresponding to the different genotypes of all the experiments of starvation resistance presented.

Figure 1A — Adult Males

	n	Median Survival	Maximum survival	$cg>w^{1118}$	$cg>p53^{H159.N}$
$cg>w^{1118}$	100	49h	67h	-	-
$cg>p53^{H159.N}$	98	37h	49h	**<0.0001**	-
$cg>p53i$	99	33h	49h	**<0.0001**	**0,0002**

Figure 2G (Chloroquine) — Adult Males

	n	Median Survival	Maximum survival	$cg>w^{1118}$	$cg>p53^{H159.N}$	Treated $cg>w^{1118}$
$cg>w^{1118}$	97	64h	80h	-	-	-
$cg>p53^{H159.N}$	50	44h	56h	**<0.0001**	-	-
Treated $cg>w^{1118}$	90	44h	56h	**<0.0001**	0,3971	-
Treated $cg>p53^{H159.N}$	103	38h	64h	**<0.0001**	0,0123	0,117

Figure 2I (Rapamycin) — Adult Males

	n	Median Survival	Maximum survival	$cg>w^{1118}$	$cg>p53^{H159.N}$
$cg>w^{1118}$	171	43h	55h	-	-
Treated $cg>w^{1118}$	193	55h	71h	**<0.0001**	-
Treated $cg>p53^{H159.N}$	198	49h	61h	**<0.0001**	**<0.0001**

Figure 4F and 7D — Adult Males

	n	Median Survival	Maximum survival	$cg>w^{1118}$	$cg>p53^{H159.N}$	$cg>Impl2$	$cg>AMPKi$
$cg>w^{1118}$	99	48h	60h	-	-	-	-
$cg>p53^{H159.N}$	70	36h	48h	**<0.0001**	-	-	-
$cg>Impl2$	99	54h	66h	**<0.0001**	**<0.0001**	-	-
$cg>Impl2, p53^{H159.N}$	99	60h	66h	**<0.0001**	**<0.0001**	0,044	-
$cg>AMPKi$	65	30h	48h	**<0.0001**	**<0.0001**	-	-
$cg>AMPKi, p53^{H159.N}$	40	36h	48h	**<0.0001**	0,2678	-	0,701

Figure 6E — Adult females

	n	Median Survival	Maximum survival	$cg>w^{1118}$	$cg>p53^{H159.N}$	$cg>Upd2i$
$cg>w^{1118}$	104	40h	60h	-	-	-
$cg>p53^{H159.N}$	76	34h	52h	**<0.0001**	-	-
$cg>Upd2i$	99	40h	52h	0,4608	**<0.0001**	-
$cg>Upd2i, p53^{H159.N}$	98	40h	52h	0,4681	**<0.0001**	**<0.0001**

Figure 6F — Adult females

	n	Median Survival	Maximum survival	$VGAT>Domei$	$VGAT>, p53^{5a14}$
$VGAT>Domei$	101	58h	82h	-	-
$VGAT>, p53^{5a14}$	100	38h	70h	**<0.0001**	-
$VGAT>Domei, p53^{5a14}$	70	50h	70h	**0,0005**	**<0.0001**

Figure S1E — Adult females

	n	Median Survival	Maximum survival	w^{1118}	$UAS\text{-}p53^{H159.N}/w^{1118}$
w^{1118}	102	44h	56h	-	-
$UAS\text{-}p53^{H159.N}/w^{1118}$	75	44h	50h	0,5424	-
$UAS\text{-}p53i/w^{1118}$	98	50h	60h	0,2083	0,1139

Figure S2K — Adult Males

	n	Median Survival	Maximum survival	$cg>w^{1118}$	$cg>p53^{H159.N}$	$cg>Atg1i$
$cg>w^{1118}$	100	49h	67h	-	-	-
$cg>p53^{H159.N}$	98	37h	49h	**<0.0001**	-	-
$cg>Atg1i$	100	33h	55h	**<0.0001**	**<0.0001**	-
$cg>Atg1i, p53^{H159.N}$	100	33h	44h	**<0.0001**	**<0.0001**	**0,0046**

Figure S4F — Adult males

	n	Median Survival	Maximum survival	$dilp2>w^{1118}$
$dilp2>w^{1118}$	97	52h	88h	-
$dilp2>p53^{H159.N}$	104	52h	83h	0,4205

Table S2. Related to Figures 1, 2, 4, 6, 7, S3, S4, S7 and STAR methods

List of primers

Gene Name	Primer sequence (Fw)	Primer sequence (Rev)
actin	CAAGTGCGAGTGGTGGAAGTT	GCAGGTGGTTCCGCTCTTT
unk	GCCCATGTGGAACCTTGC	GCGCCGAGGAACGTGTTA
InR	GCTGTCAAGCAAGCAGTGAA	TCTTTTTACCCGTCGTCTCC
4EBP	AACCCTCTACTCCACCACTC	CAATCTTCAGCGACTTGG
dilp2	GTATGGTGTGCGAGGAGTAT	TGAGTACACCCCCAAGATAG
dilp5	AGTTCTCCTGTTCCTGATCC	CAGTGAGTTCATGTGGTGAG
Upd2	CGGAACATCACGATGAGCGAAT	TCGGCAGGAACTTGTACTCG
ccha2	AAACAGCAACAGCAGCAAAC	AGGACCACGGTGCAGATAAC
ccha1	AGTGCAGTTGGACTTTGGTAGTGT	AGGGATGCTGTTTAGCATCTATGAC
gbp1	ATCCTACCGCTGGTCTTCCTC	CTCCAGCAATATTCGGTTGTC
gbp2	CGCCTCCTTCGTATTATCCAG	CCAGATGGTTGTGGTCTATTG
GFP	CCCGACAACCACTACCTGA	CGGTCACGAACTCCAGCA
Sesn	TTCACCAGATACGGACACTGA	TCCGCTGCCTAACGATTACAG
TSC2	GAGCCGTTTATAGAAGCTCAAGG	GCTGCACAACTTCAATCTGGA
sun	ATGACTGCCTGGAGAGCTG	GTGAACTTCACATGGCTCGC